Research Square

Preprints are preliminary reports that have not undergone peer review.
They should not be considered conclusive, used to inform clinical practice,
or referenced by the media as validated information.

Spatial and decadal variability of drought in Burkina Faso and associated teleconnections: a multi-scale analysis using the SPI and SPEI (1981–2025)

Joseph YAMÉOGO

josephyameogo10@gmail.com

Ziniaré University Centre/Joseph KI-ZERBO University

Songanaba Rouamba

Norbert ZONGO University

Research Article

Keywords: drought, SPI, SPEI, regionalization, decadal variability, teleconnections, wavelets, Burkina Faso

Posted Date: November 20th, 2026

DOI: https://doi.org/10.21203/rs.3.rs-11495353/v1

License: This work is licensed under a Creative Commons Attribution 4.0 International License.
Read Full License

Additional Declarations: No competing interests reported.

Spatial and decadal variability of drought in Burkina Faso and associated teleconnections: a multi-scale analysis using the SPI and SPEI (1981–2025)

Joseph YAMÉOGO

Department of Human and Social Sciences, Ziniaré University Centre/Joseph KI-ZERBO University, Ouagadougou, Burkina Faso

mail : josephyameogo10@gmail.com

Songanaba ROUAMBA

Department of Geography, Norbert ZONGO University, Koudougou, Burkina Faso

mail: songanaba@gmail.com

Abstract

In Burkina Faso, drought is generally described at a national level, as if it were evolving uniformly. This study has three objectives for the period from 1981 to 2025: to delineate homogeneous drought regions; to characterise the decadal variability of drought within each of these regions, as well as the proportion attributable to evaporation demand; and to identify the associated teleconnections and their stability over time. Six indices (3-, 6- and 12-month SPI and SPEI), calculated for the 47 provinces using CHIRPS precipitation data and AgERA5 reference evapotranspiration, enable these three objectives to be achieved. A principal component analysis with Varimax rotation, followed by clustering using Ward's method, distinguishes four regions: the north-eastern Sahel, the central-west, the central-east and the south-western Sudan, the boundaries of which do not correspond to the administrative divisions of 2025. The 1981–1990 decade was, on average, the driest everywhere. In the north and centre, drought subsequently decreased sharply, with the six indices increasing by between 1.09 and 1.82 standard deviations between 1981–1990 and 2011–2020. In the south-west, the increases (+0.46 to +0.93) are not significant for any index, as evaporation demand offsets between 18 per cent (3 months) and 44 per cent (12 months) of the increase due to rainfall; in the far south-west, rainfall itself has not recovered. The Mediterranean Sea surface temperature is the only oceanic index significantly linked to drought during the rainy season in all four regions ($r = +0.46$ to $+0.53$ for SPI-3 and SPEI-3). The Gulf of Guinea plays a role only in the south-west, independently of ENSO, although this link is tenuous. The link with ENSO, which was clear until the mid-2000s, has since weakened.

Keywords: drought, SPI, SPEI, regionalization, decadal variability, teleconnections, wavelets, Burkina Faso

1 Introduction

The droughts of the 1970s and 1980s made the Sahel one of the regions of the world where rainfall variability has been most extensively studied. The partial recovery in rainfall observed since the 1990s [1–3] has been neither uniform nor regular: more pronounced in the central Sahel than in the western Sahel [1], it has been accompanied by more intense and erratic rainfall [4, 5]. For Burkina Faso, several recent studies have described this trend in terms of cumulative rainfall totals and their distribution, extreme rainfall events and anomaly indices [6–10]. Whilst these studies reveal a marked contrast between the Sahelian region in the north and the Sudanese region in the south, they generally remain at the scale of climatic zones or the country as a whole.

However, drought is primarily a regional phenomenon: a dry year in the north may be normal in the south-west, and the provinces affected by prolonged droughts vary from one decade to the next. To better understand this diversity, drought geography has long employed regionalisation, which groups together areas where indices vary in a coordinated manner, usually by means of principal component analysis supplemented by cluster analysis [11–14]. In West Africa, this has enabled the identification of specific drought regimes in the eastern Sahel, the western Sahel, the savannahs and the Guinean coast [15]. No regionalisation of this kind has, however, been undertaken in Burkina Faso at the provincial scale, although it is at this scale that agricultural-season monitoring and public action are organised.

The choice of index is just as important as that of the spatial scale. The Standardised Precipitation Index (SPI; [16]) is based solely on precipitation, whilst the Standardised Precipitation-Evapotranspiration Index (SPEI; [17]) also incorporates atmospheric evaporation demand, which increases as the climate warms. Calculated at different time scales, these two indices reflect the different forms of drought that have long been distinguished on the basis of their impacts [18, 19]: over a three-month period, they describe monsoon-season drought, to which crops and pastures are exposed, and over a twelve-month period, annual drought, on which the filling of reservoirs and the recharge of groundwater aquifers depend. A given region may therefore be spared the former whilst suffering from the latter. Finally, Sahelian drought depends on ocean conditions, with ENSO, the tropical Atlantic and the Mediterranean modulating the West African monsoon [20–22] through relationships that evolve over time [23]. Given that the effects of these oscillations also vary from one location to another, the Gulf of Guinea, for example, leads to increased rainfall along the coast but reduced rainfall in the Sahel [24, 25], it is likely that each drought-prone region has its own teleconnections.

In this study, we examine the spatial and decadal variability of drought in Burkina Faso between 1981 and 2025, as well as the associated teleconnections. We have three objectives:

(1) to delineate the regions where drought varies in a homogeneous manner, hereinafter referred to as ‘drought regions’;

(2) to characterise, within each of these regions, the decadal variability of drought and the proportion accounted for by evaporative demand;

(3) to identify the teleconnections associated with drought in each region and assess their stability over time.

2 Study area, data and methods

2.1 Study area

The country of Burkina Faso, with an area of approximately 274,000 km², is situated between 9.4° and 15.1° north latitude. Divided between a Sahelian zone in the north and a Sudanese zone in the south, it is crossed by a rainfall gradient extending from the south-west to the north-east: average annual rainfall exceeds 1,050 mm in Poni, Comoé and Léraba, but is less than 400 mm in Oudalan (Fig. 1). The rainy season lasts from May to October in the south-west, but is limited to the period from July to September in the north. Since July 2025, the country has comprised 17 regions, 47 provinces and 351 municipalities; this division serves as the framework here, with indices calculated for the 47 provinces and the resulting drought zones compared with the 17 administrative regions.

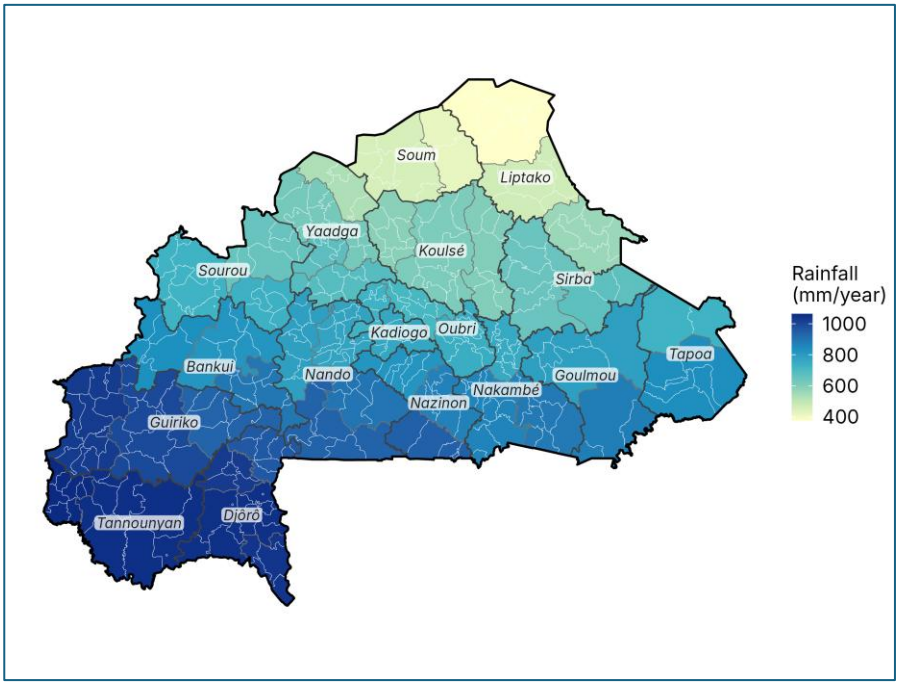


Fig. 1 Study area: mean annual rainfall of the 47 provinces (1981–2025) and 2025 administrative divisions. Sources: CHIRPS v2.0 [26]; administrative boundaries from OCHA [27]. Thin lines: communes and provinces; thick lines: administrative regions (names in italics).

2.2 Data

Rainfall data were obtained from CHIRPS v2.0 [26]: after calculating the average by province, the daily values from this product – which accurately reproduces the cumulative rainfall observed in Burkina Faso [28] – were then totalled on a monthly basis. Reference evapotranspiration (ET0) was derived from AgERA5 [29], a dataset derived from the ERA5 reanalysis, in which it is calculated using the FAO's Penman-Monteith formula [30]. The ten ocean indices selected relate to the Pacific, the Atlantic and the Mediterranean. For the Pacific, these are the Niño 3.4 index [31], the Southern Oscillation Index (SOI) and the Pacific Decadal Oscillation (PDO; [32]). The Atlantic is represented by the Atlantic Multidecadal Oscillation (AMO; [33]), the North Atlantic Oscillation (NAO; [34]), temperatures in the North (TNA) and South (TSA) Tropical Atlantic [35], the Atlantic Meridional Mode (AMM; [36]) and the Gulf of Guinea Index (ATL3; [37]), to which is added the Mediterranean Sea surface temperature (MED). The last two indices were calculated using the ERSSTv5 reconstruction [38], whilst the others were derived from NOAA's PSL. The administrative boundaries (municipalities, provinces and regions) are those of OCHA [27] and correspond to the 2025 divisions (Table 1).

Table 1 Data used

Data	Source	Variable	Resolution	Period
Rainfall	CHIRPS v2.0 [26]	Monthly total, provincial mean	0.05°, 47 provinces	1981–2025
ET0	AgERA5 [29]	Penman-Monteith ET0, provincial mean	0.1°, 47 provinces	1981–2025
Ocean indices	NOAA PSL; ERSSTv5 [38]	Niño 3.4, SOI, PDO, AMO, NAO, TNA, TSA, AMM, ATL3, MED	Monthly index	1981–2025 (AMO: to 2022)
Boundaries	OCHA [27]	Country, 17 regions, 47 provinces, 351 communes	Vector	2025 divisions

2.3 Drought indices

The climatic water balance of month *t* is the difference between rainfall and reference evapotranspiration (Eq. (1)):

$$D_t = P_t - ET0_t \tag{1}$$

The *k*-month SPEI is obtained by accumulating this balance over the last *k* months, fitting a log-logistic distribution to the accumulated value for each calendar month, and then transforming its probability into a standard normal deviate (Eq. (2)):

$$\mathrm{SPEI}_t = \Phi^{-1}\left(F\left(\sum_{j=0}^{k-1} D_{t-j}\right)\right) \tag{2}$$

where F is the fitted distribution function and Φ is that of the standard normal distribution. As in the SPEI package, the fit is based on the L-method of moments [39, 40]. For the SPI, the same procedure is applied solely to precipitation using a gamma distribution [16], and the probability of a zero total is estimated according to Stagge et

al. [41]. As all distributions are fitted to the period 1981–2025, each index represents a deviation from the mean for that period. Both indices are calculated on 3-, 6- and 12-month scales; in the monthly statistics, the 12-month scale covers the whole year, whilst the shorter scales are limited to the rainy season, namely July to October for the 3-month scale and September and October for the 6-month scale. An annual value is also assigned to each scale: the September index for the 3-month period (July–September), the October index for the 6-month period (May–October) and the December index for the 12-month period (calendar year). A month is classified as dry when its index is below −1. The six indices (SPI-3, SPI-6, SPI-12, SPEI-3, SPEI-6 and SPEI-12) serve three purposes: at the same scale, the difference between the SPI and the SPEI makes it possible to isolate the effect of evapotranspiration, whilst across scales, the comparison helps to distinguish between monsoon-season drought and annual drought.

2.4 Delineation of drought regions

For each of the six indices, the matrix of monthly values (months × 47 provinces) was submitted to a standardised principal component analysis (PCA), the number of components, between two and six, being set by the Kaiser criterion (eigenvalue greater than 1). The loadings were then rotated with the varimax method [42], which attaches each province to a single component and thus eases regional interpretation [11]. Ward's agglomerative hierarchical clustering [43] was applied to the rotated loadings to group the provinces. The number of clusters, set between three and six, is selected using the mean silhouette width [44], which contrasts, for each province *i*, the mean distance *a*(*i*) to the other members of its cluster with the mean distance *b*(*i*) to the members of the nearest cluster (Equation (3)):

$$s(i) = \frac{b(i) - a(i)}{\max(a(i), b(i))} \tag{3}$$

A silhouette close to 1 denotes well-separated clusters, whereas a value close to 0 denotes overlapping clusters. So as not to fragment the country without real gain, we retain the smallest number of clusters whose silhouette lies within 0.01 of the maximum. The SPEI-12 regionalisation, which combines rainfall and evaporative demand over the full year, serves as the reference for objectives 2 and 3; its agreement with the regionalisations derived from the other five indices is measured by the adjusted Rand index [45], which equals 1 for identical partitions and 0 for agreement due to chance alone. Finally, the regions obtained are overlaid on the 17 administrative regions and the 351 communes, in area and in number.

2.5 Decadal variability and share of evaporative demand

For each region, the rainfall and ET0 of its provinces were averaged and the six indices recomputed from these means, so that every decadal statistic refers to the six regional indices. The period was split into five decades (1981–1990, 1991–2000, 2001–2010, 2011–2020 and 2021–2025), the last being incomplete. For each decade, the proportion of dry months is supplemented, in accordance with run theory [46], by the number of drought episodes, their duration and their severity, the latter corresponding to the sum of deviations below the threshold of −1; the extent of the drought corresponds to the proportion of provinces in the region whose index is below −1. The Kruskal-Wallis test, applied to annual values, compares the decades, whilst a permutation test (5,000 draws) on the difference in means assesses the difference between the periods 1981–1990 and 2011–2020; this difference is also calculated for each of the 47 provinces (2,000 draws). Finally, at each scale, the ratio (ΔSPI − ΔSPEI) / ΔSPI, that is, the proportion of the increase in the SPI that is not reflected in the SPEI, indicates the extent to which evaporation demand reduces the increase attributable to precipitation.

2.6 Teleconnections and their stability over time

Three approaches, each applied to the six drought indices, were used to investigate the links with the oceans. The first establishes a correlation between the annual values, from which the linear trend has been removed – and the ocean indices averaged over the same months, namely July–September for the quarterly scale, May–October for the half-yearly scale and the calendar year for the annual scale. As the annual time series are autocorrelated, significance is assessed using an effective sample size [47] (Equation (4)):

$$n_{\text{eff}} = n\frac{1 - \rho_x\rho_y}{1 + \rho_x\rho_y} \tag{4}$$

where ρx and ρy are the first-lag autocorrelations of the two time series. For each drought index, the false discovery rate [48] is used to correct the 40 tests (4 regions × 10 oceanic indices). We examine the stability of the relationships on a decade-by-decade basis and over 15-year sliding windows. This approach is supplemented by excluding the year 2015, which was marked by a strong El Niño, thereby allowing us to assess the sensitivity of the ENSO link to that particular year, as well as by a partial correlation, with the Niño 3.4 index removed from both time series, which tests the independence of the Gulf of Guinea link from ENSO. Secondly, ocean indices for dry years – defined as those in the lower tertile of annual values – are compared, in composite form, with those for wet years – defined as those in the upper tertile – with the difference subjected to a permutation test. Finally, following Grinsted et al. [49], we calculated, using a Morlet wavelet [50], the wavelet coherence between the monthly

time series of each of the six regional indices and the seven oceanic indices (Equation (5)):

$$R_n{}^2(s) = \frac{| S\left(s^{-1} W_n{}^{XY}(s)\right) |^2}{S\left(s^{-1} | W_n{}^X(s) |^2\right) \cdot S\left(s^{-1} | W_n{}^Y(s) |^2\right)} \quad (5)$$

where W denotes the wavelet transforms, s the scale, and S smoothing in both time and scale. The 95 per cent threshold is determined from 200 simulations of red noise exhibiting the same autocorrelations as the observed time series. The proportion of significant cells located outside the cone of influence summarises the coherence in two period bands, 2–7 years and 8–16 years, over the entire period and for each decade, provided that the decade in question contains at least 100 cells outside the cone. As the SPI index is not defined during the dry season months, when most cumulative values are zero, a neutral value of 0 was assigned to them for the wavelet calculation.

All figures and tables cover the six indices; in the text, the SPI-3, which is representative of drought during the wet season, and the SPEI-12, which accounts for annual drought by including evaporative demand, are commented on first. All calculations were programmed in R, and the indices and wavelets were verified against benchmark implementations in Python (lmoments3, scipy, pycwt), with which they agree.

3 Results

3.1 Four homogeneous drought regions

3.1.1 From the Sahelian north-east to the Sudanian south-west

For SPEI-12, four principal components account for 90.2 per cent of the variance across the 47 provinces, and the silhouette analysis highlights four regions (average silhouette value of 0.36), which align along the rainfall gradient whilst crossing it from east to west (Fig. 2 and Table 2). In the north-east, region R1 comprises seven Sahelian provinces, from Oudalan to Namentenga; it receives 497 mm per year and is subject to the highest evaporative demand (2,493 mm). Region R2, in the central-west, covers twelve provinces, from Loroum and Yatenga to Mouhoun and Balé, with an annual rainfall of 710 mm. Region R3, in the central-east, is the largest, comprising nineteen provinces stretching from Kadiogo to Gourma and Kompienga, accounting for 37 per cent of the territory – and receiving 801 mm of rainfall. Finally, Region R4, in the south-west, comprises nine Sudanese provinces, from Houet to Poni; it is the wettest (1,017 mm) and least affected by evaporation (1,997 mm).

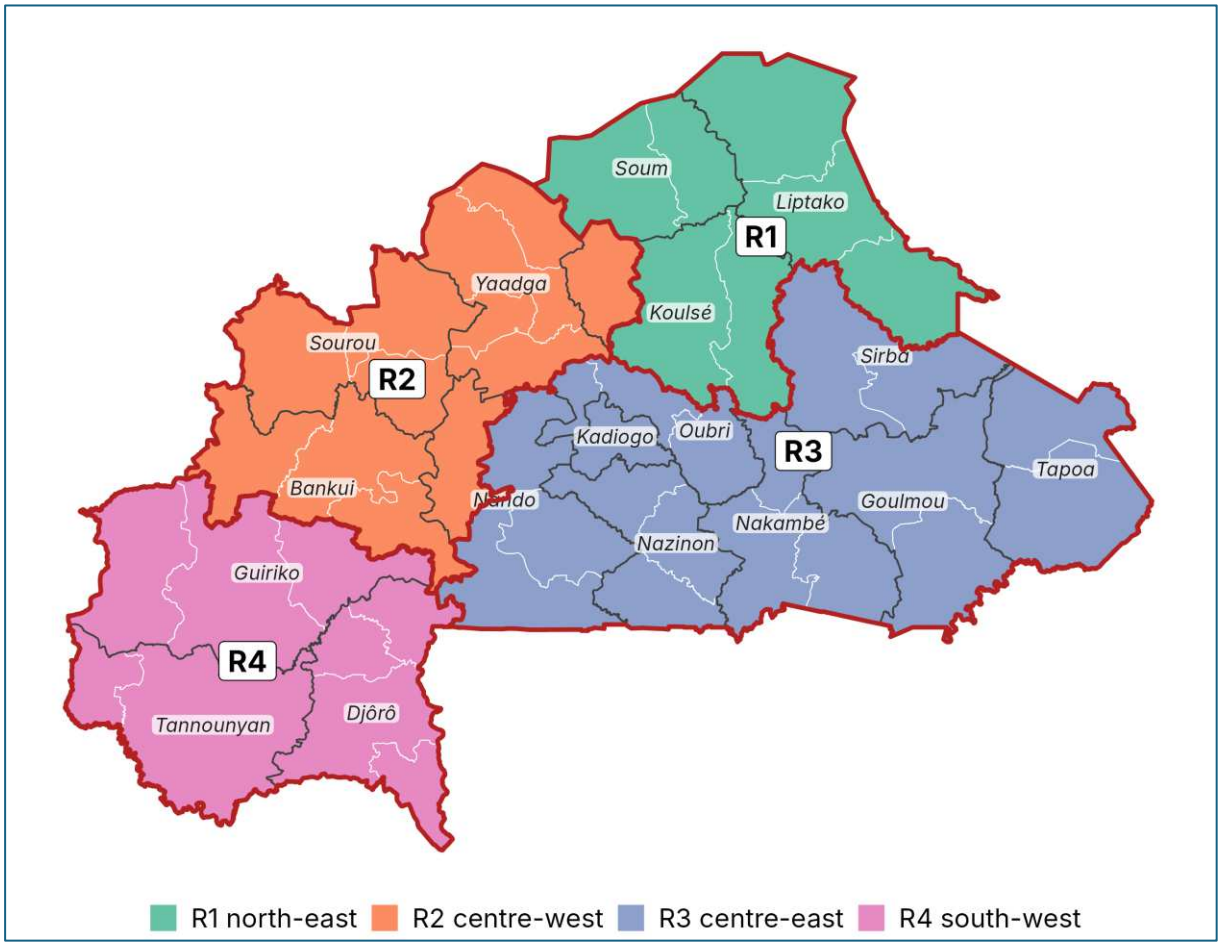


Fig. 2 Homogeneous drought regions delineated from the SPEI-12, and administrative regions. Red outlines: drought regions; grey lines: administrative regions (names in italics). PCA with varimax rotation, then Ward clustering. Sources: CHIRPS v2.0; AgERA5 [29]; OCHA.

Even before clustering, the four rotated components – numbered in the order preceding the rotation – outline the contours of these regions. The highest loadings of the first component, which explains 28.5 per cent of the variance, are found in the centre and east (up to 0.83 at Kourittenga); the second (17.9 per cent) peaks in the south-west (0.92 in Poni), the third (22.7 per cent) in the centre-west (0.74 in Mouhoun) and the fourth (21.1 per cent) in the north-east (0.85 in Oudalan). Only the absolute value of the loading coefficients, the sign of which is arbitrary, indicates a province's weight within a component. With the exception of Sissili, each province has a loading coefficient of at least 0.6 on one of the components. Common loadings are limited to the contact zones: between the south-west and the centre-west (Kénédougou, Tuy), between the centre-west and the north-east (Bam, Loroum) and between the south-west and the centre-east (Sissili), intermediate cases which the clustering merely confirms.

Within the same region, the provinces show very similar trends, with the average correlation of their monthly SPEI-12 ranging from 0.76 in the south-west to 0.90 in the north-east; this cohesion therefore decreases with rainfall, reflecting the greater diversity of conditions in the Sudanese zone. The drought regions do not, however, correspond to administrative divisions (Table 2). Whilst the south-west corresponds

exactly to the regions of Guiriko, Tannounyan and Djôrô, and the north-east comprises Liptako, Soum and 80 per cent of Koulsé, Koulsé and Nando, on the other hand, are spread across two drought regions, and region R3 comprises eight administrative regions, from Goulmou to Kadiogo, and alone accounts for 131 of the country's 351 municipalities.

Table 2 Characteristics of the four drought regions (reference: SPEI-12)

Region	Prov.	Area (km²; % of country)	Comm.	Administrative regions	Rainfall (mm/yr)	ET0 (mm/yr)	Internal r
R1 north-east	7	51,301; 18.7	45	Liptako, Soum, Koulsé (80%)	497	2,493	0.90
R2 centre-west	12	60,287; 22.0	97	Bankui, Sourou, Yaadga, Nando (24%), Koulsé (20%)	710	2,228	0.89
R3 centre-east	19	102,303; 37.3	131	Goulmou, Tapoa, Nakambé, Sirba, Nazinon, Oubri, Kadiogo, Nando (77%)	801	2,185	0.83
R4 south-west	9	60,377; 22.0	78	Guiriko, Tannounyan, Djôrô	1,017	1,997	0.76

Percentages in brackets: share of the area of the administrative region lying within the drought region. Internal r: mean correlation between the monthly SPEI-12 of the provinces of the region. Prepared by J. Yaméogo, 2026.

3.1.2 A stable delineation in the south-west, more fluctuating in the centre-east

Although they are not identical, the regionalisations obtained from the other five indices are similar to the reference ones (Fig. 3), with the adjusted Rand index ranging from 0.42 (SPEI-3) to 0.67 (SPI-6). They comprise between three (SPEI-3) and five regions (SPI-3 and SPI-6), with an explained variance of 86–90 per cent and a silhouette coefficient of 0.33–0.40. The SPEI-3 distinguishes only three clusters: a vast northern region, the south-east and the south-west; the SPI-3 and SPI-6 indices, by contrast, isolate the far east (Gourma, Kompienga, Koulpelogo, Dyamongou and Gobnangou), where seasonal rainfall patterns evolve partly independently of those in the rest of the centre-east.

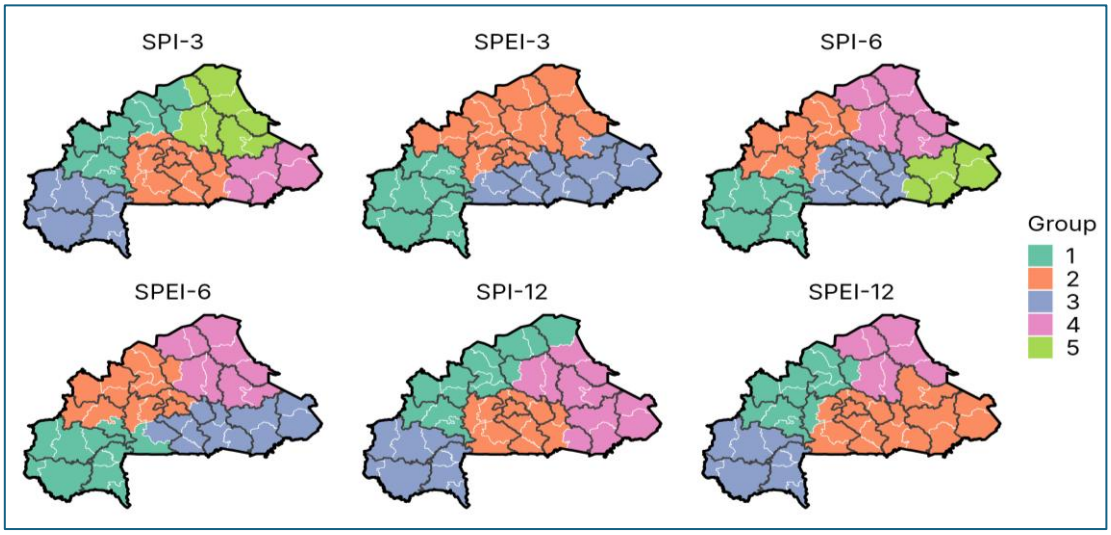


Fig. 3 Regionalization of drought by index and time scale. Group numbers are specific to each index; colours do not correspond from one map to another. Sources: CHIRPS v2.0; AgERA5; OCHA.

Nevertheless, one pattern emerges across all six regional groupings: that of the south-west, whose nine provinces always belong to the same group, regardless of the index or time scale used, with this group extending to a maximum of three neighbouring

provinces. The north-east is almost as stable, as its seven provinces remain grouped together for four out of six indices. The centre-east, on the other hand, is the most fragile region: depending on the index, only 63 to 74 per cent of its provinces remain in the same group, with its easternmost part tending to break away. Ultimately, drought in Burkina Faso is organised around two stable poles, the Sahelian north-east and the Sudanese south-west – with these poles separated by a vast central zone whose internal boundaries depend on the index and the timescale.

3.2 Contrasting decadal variability among regions

3.2.1 A dry 1980s everywhere, then a clear decline in the north and centre

All six indices show the same general trend. In all four regions and for each of the six indices, the annual average reached its lowest point between 1981 and 1990, a decade which also accounted for the highest proportion of dry months, except in the south-west, where the decade 2001–2010 equalled or exceeded this for the three SPEI indices (Fig. 4) . In the north-east and centre-west, at least half of the months were dry during that period, regardless of the index, ranging from 50 to 53 per cent for the SPEI and 52 to 70 per cent for the SPI; the centre-east was slightly less affected (30 to 55 per cent), and the south-west significantly less so (25 to 32 per cent).

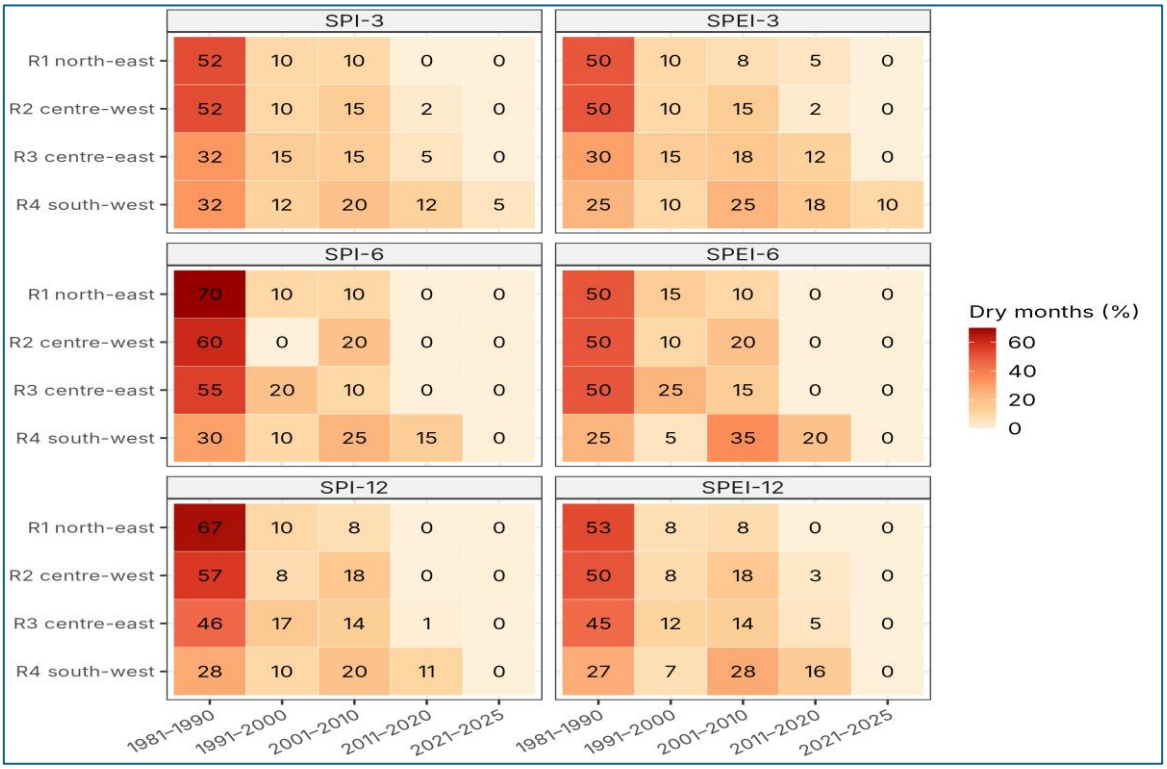


Fig. 4 Share of dry months (index < −1) by region, index and decade. 3- and 6-month scales: rainy-season months only (July–October and September–October). Sources: CHIRPS v2.0; AgERA5.

The time scale changes the shape of episodes more than their chronology (Table 3). While at 3 months the drought of the 1980s fragments, in the north-east and centre-west, into eight or nine episodes of two to three months, at 12 months it resolves into

a few very long episodes, namely four episodes of 19 months on average for the SPI-12 in the north-east and two of 15 months in the south-west.

Table 3 Number of drought episodes and mean duration (months, in brackets) by region and decade, for the six indices

Region	Index	1981–1990	1991–2000	2001–2010	2011–2020	2021–2025
R1 north-east	SPI-3	8 (2.6)	3 (1.3)	2 (2.0)	0	0
	SPEI-3	8 (2.5)	3 (1.3)	3 (1.0)	2 (1.0)	0
	SPI-6	7 (2.0)	1 (2.0)	1 (2.0)	0	0
	SPEI-6	5 (2.0)	2 (1.5)	1 (2.0)	0	0
	SPI-12	4 (19.2)	2 (4.0)	1 (9.0)	0	0
	SPEI-12	5 (12.0)	3 (2.7)	2 (4.5)	0	0
R2 centre-west	SPI-3	9 (2.3)	4 (1.0)	4 (1.5)	1 (1.0)	0
	SPEI-3	8 (2.5)	4 (1.0)	4 (1.5)	1 (1.0)	0
	SPI-6	6 (2.0)	0	2 (2.0)	0	0
	SPEI-6	5 (2.0)	1 (2.0)	2 (2.0)	0	0
	SPI-12	5 (13.4)	3 (1.7)	3 (7.0)	0	0
	SPEI-12	8 (7.4)	3 (2.0)	4 (5.2)	2 (2.0)	0
R3 centre-east	SPI-3	5 (2.6)	3 (2.0)	5 (1.2)	2 (1.0)	0
	SPEI-3	4 (3.0)	3 (2.0)	5 (1.4)	4 (1.2)	0
	SPI-6	6 (1.8)	2 (2.0)	2 (1.0)	0	0
	SPEI-6	5 (2.0)	3 (1.7)	2 (1.5)	0	0
	SPI-12	6 (9.0)	3 (7.7)	2 (5.0)	1 (1.0)	0
	SPEI-12	4 (13.2)	4 (4.2)	4 (2.5)	2 (3.0)	0
R4 south-west	SPI-3	5 (2.6)	3 (1.7)	3 (2.7)	3 (1.7)	1 (1.0)
	SPEI-3	5 (2.0)	3 (1.3)	4 (2.5)	4 (1.8)	2 (1.0)
	SPI-6	3 (2.0)	1 (2.0)	3 (1.7)	2 (1.5)	0
	SPEI-6	3 (1.7)	1 (1.0)	5 (1.4)	2 (2.0)	0
	SPI-12	2 (15.0)	1 (12.0)	2 (12.0)	2 (6.5)	0
	SPEI-12	2 (14.5)	2 (4.0)	5 (6.6)	4 (4.8)	0

Episode: sequence of months during which the regional index remains below −1 (run theory), assigned to the decade in which it begins. 3- and 6-month scales: rainy-season months only. Prepared by J. Yaméogo, 2026.

In the north and centre, all indicators therefore show a marked decline in drought. The proportion of dry months in the north-east fell to 8–15 per cent between 1991 and 2000, then to 0–5 per cent between 2011 and 2020. In both the central-west and the central-east, a partial resurgence was observed between 2001 and 2010 (10–20 per cent of months classified as dry, depending on the index), followed, between 2011 and 2020, by an almost complete decline (0–5 per cent of months classified as dry, with the exception of the SPEI-3 index for the central-east, which stood at 12 per cent). Between 1981–1990 and 2011–2020, the increase in the six annual indices across these three regions ranged from 1.09 to 1.82 standard deviations and was statistically significant everywhere (Table 4); the Kruskal–Wallis test also confirms a difference between the decades (p ranging from 0.001 to 0.034), with the central-eastern SPEI-3 being the sole exception (p = 0.066). At all time scales, the SPI shows a greater increase than the SPEI, and the difference between the two, which measures the proportion by which evaporative demand reduces the increase attributable to

precipitation, accounts for 12–16 per cent of the SPI's increase at 3 and 6 months and 15–20 per cent at 12 months.

Table 4 Difference in annual SPI and SPEI between 2011–2020 and 1981–1990 (standard deviations)

Region	SPI-3	SPEI-3	SPI-6	SPEI-6	SPI-12	SPEI-12
R1 north-east	+1.70 (0.001)	+1.44 (0.002)	+1.82 (<0.001)	+1.53 (<0.001)	+1.81 (<0.001)	+1.45 (0.001)
R2 centre-west	+1.56 (0.003)	+1.34 (0.005)	+1.70 (0.001)	+1.44 (0.001)	+1.71 (<0.001)	+1.40 (0.001)
R3 centre-east	+1.24 (0.013)	+1.09 (0.021)	+1.48 (0.002)	+1.31 (0.002)	+1.49 (0.001)	+1.27 (0.004)
R4 south-west	+0.57 (0.279)	+0.46 (0.351)	+0.84 (0.089)	+0.64 (0.158)	+0.93 (0.061)	+0.52 (0.245)

In brackets: *p*-value of the permutation test (5,000 draws) on the difference of means. Annual values: September (3 months), October (6 months), December (12 months). Share of the SPI gain taken back by evaporative demand, (SPI difference − SPEI difference) / SPI difference: 12 to 15% (3 months), 12 to 16% (6 months) and 15 to 20% (12 months) from R1 to R3; 18, 24 and 44% in R4.

3.2.2 The south-west: drought persisting until 2020

The trend observed in the south-west is quite different, and the six indices describe it consistently. Following a wet decade from 1991 to 2000 (5 to 12 per cent of months were dry, depending on the index), drought re-emerged there between 2001 and 2010. It was then just as frequent, if not more so, than in the 1980s according to the SPEI (25–35 per cent of months were dry, compared with 25–27 per cent), and slightly less frequent according to the SPI (20–25 per cent, compared with 28–32 per cent), and the SPEI-12 recorded five episodes there, compared with two in the 1980s. Far from abating, drought persisted there between 2011 and 2020 (11–15 per cent of months were dry according to the SPI, 16–20 per cent according to the SPEI), whilst it had almost disappeared elsewhere. In both the 2001–2010 and 2011–2020 periods, the SPEI thus indicates more dry months than the SPI in the south-west at all scales, a sign that evaporative demand there exacerbates the drought more than precipitation alone would suggest.

The maps drawn up by province clearly illustrate this (Fig. 5). Generally present in 1981–1990, drought was more pronounced in the north at that time, with the proportion of dry months varying, depending on the index, from 18 to 26 per cent in the least affected provinces to 55 to 70 per cent in the most affected. It shifted towards the south-west in 2001–2010, a decade during which the most affected province was in this region for all six indices, sometimes tied with a neighbouring province (Houet for the SPI-12, SPEI-6 and SPEI-12, with 31 to 40 per cent of dry months). Between 2011 and 2020, the south-western provinces recorded an average of between 13 and 21 per cent of dry months depending on the index, compared with 0 to 10 per cent in the other

regions, and most of the ten most affected provinces (six to nine depending on the index) are located there.

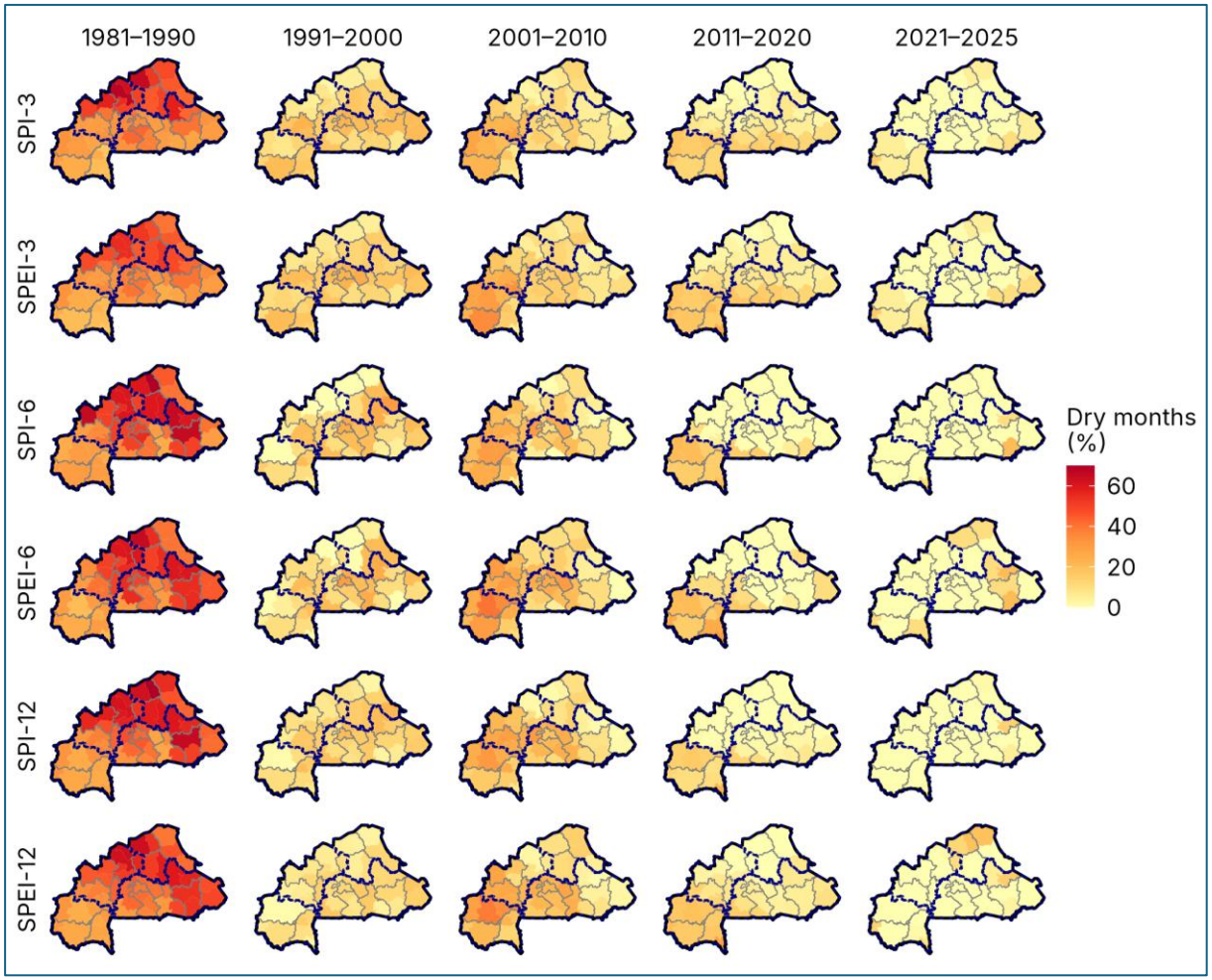


Fig. 5 Share of dry months (index < −1) by province and decade, for the six indices. 3- and 6-month scales: rainy-season months only. Dashed blue lines: drought regions; grey lines: administrative regions. Sources: CHIRPS v2.0; AgERA5; OCHA.

None of the six indices showed a significant increase in the south-west between 1981–1990 and 2011–2020 (p ranging from 0.06 to 0.35; Table 4), and these increases, ranging from +0.46 (SPEI-3) to +0.93 (SPI-12), remain lower than those in other regions. The proportion accounted for by evaporation demand increases with the time scale (18 per cent over 3 months, 24 per cent over 6 months, 44 per cent over 12 months), whilst it is limited to 12–20 per cent elsewhere. This distinctive feature is also evident in the annual values (Fig. 6): the 10-year average of the SPEI-12 for the south-west, which was negative between 2001 and 2010 (−0.25), is barely positive between 2011 and 2020 (+0.02), whilst it ranges between +0.38 and +0.54 in the other three regions. The ranking of the years confirms this. Of the fifteen driest years in the south-west according to the SPEI-12, nine occurred after 2000 (2001, 2002, 2004, 2005, 2007, 2008, 2011, 2013 and 2017), compared with five or six in the other regions. In the north-east, two recent years, 2021 and 2023, also feature amongst the fifteen driest. Whilst generally wet at regional level, the 2021–2025 period shows only a few

dry months in the south-west on a quarterly basis (5 per cent for the SPI, 10 per cent for the SPEI).

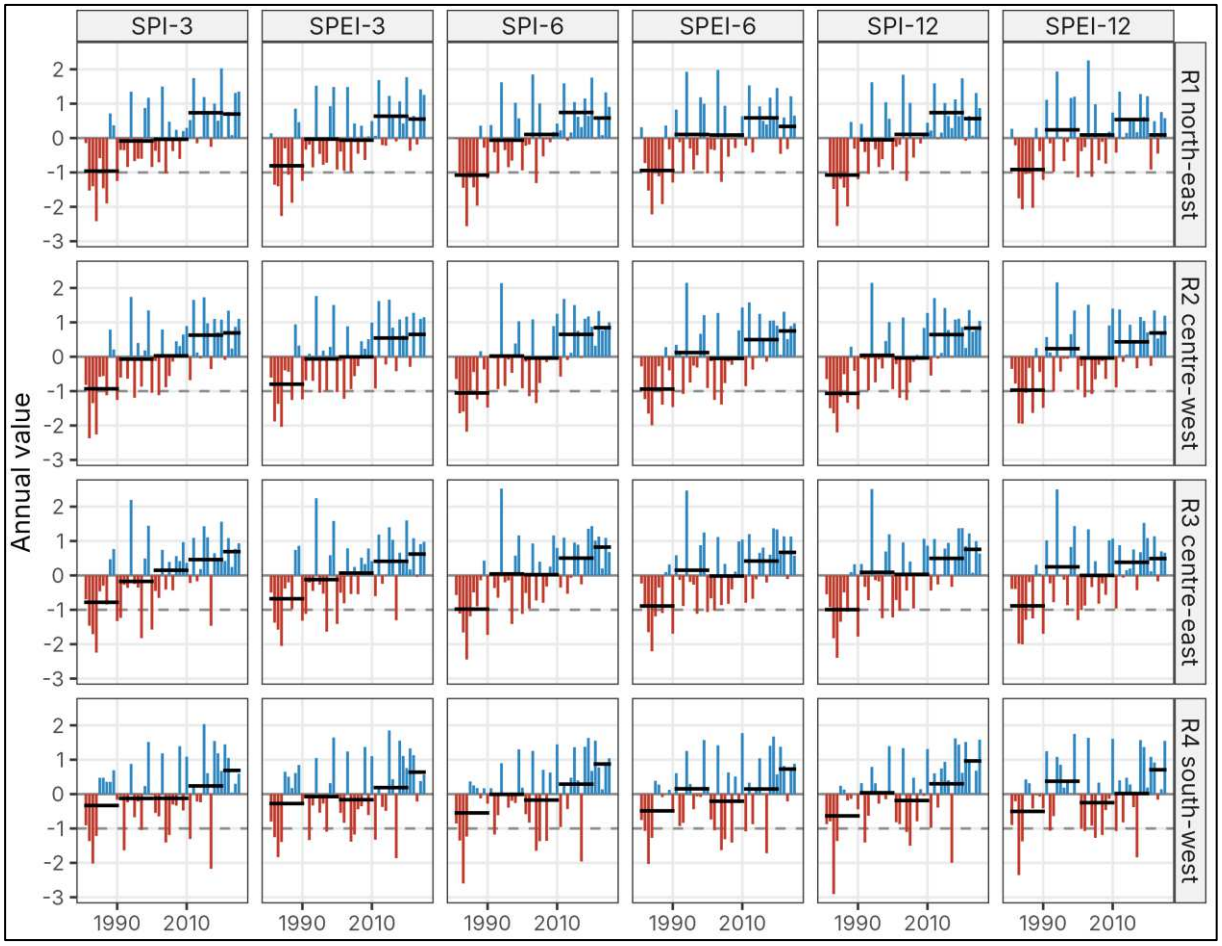


Fig. 6 Annual SPI and SPEI by region (September values for the 3-month scale, October for 6 months and December for 12 months) and decadal means. Horizontal lines: decadal means; dashes: threshold of −1. Sources: CHIRPS v2.0; AgERA5.

Calculating the differences province by province makes it possible to identify the geographical distribution of this exception (Fig. 7). Significant in 43 of the 47 provinces for the SPI-6 and SPI-12, the gains are significant in 40 provinces for the SPEI-6, in 38 for the SPEI-12 and in only 32 and 33 for the quarterly indices, which are more sensitive to individual years. In the south-west, only 1 to 3 out of 9 provinces recorded a significant increase for the SPEI, and 2 to 5 for the SPI. Two contrasting situations exist there. In the north of the region (Houet, Bougouriba, Ioba, Kénédougou, Tuy), rainfall has recovered, as shown by an SPI-12 rising from 1.07 to 1.28 standard deviations, but evaporative demand offsets a quarter or a third of this gain (25 to 35 per cent over a 12-month period). In the far south-west (Comoé, Léraba, Noumbiel, Poni), where even rainfall has not recovered, no index has shown significant improvement: the SPI-12 has risen only from +0.07 to +0.59, whilst the SPEI-12 remains stable (from −0.18 to +0.18).

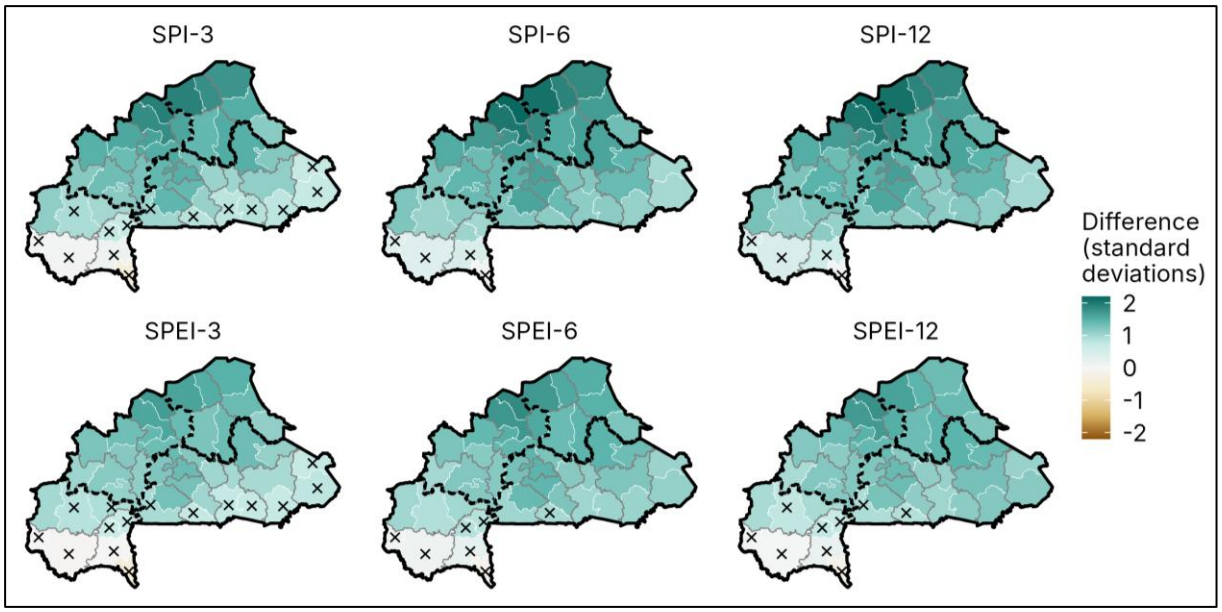


Fig. 7 Difference in annual SPI and SPEI between 2011–2020 and 1981–1990, by province. Crosses: non-significant difference (permutation test, $p \geq 0.05$); dashed lines: drought regions; grey lines: administrative regions. Sources: CHIRPS v2.0; AgERA5; OCHA.

3.3 Common, regional and changing teleconnections

3.3.1 The Mediterranean: a link common to all regions

After adjusting for multiple testing, the surface temperature of the Mediterranean Sea is the only oceanic index showing a significant correlation with drought over the entire period (Fig. 8). This link, which is significant across all four regions for both quarterly indices, is reflected in very similar correlations (+0.50 to +0.53 for SPEI-3, +0.46 to +0.51 for SPI-3). It weakens as the time scale increases, falling to +0.34 to +0.46 over 6 months, values that do not withstand correction, and then to +0.13 to +0.33 over 12 months. A wetter rainy season across the country is therefore accompanied by a warmer-than-usual Mediterranean Sea in July-September, and this relationship is as clear in precipitation alone (SPI) as it is in the water balance (SPEI). The remaining links are not very strong.ENSO is negative for the quarterly indices in all four regions

(r = −0.12 to −0.28), it virtually disappears at the 6- and 12-month time scales (−0.12 to +0.08).

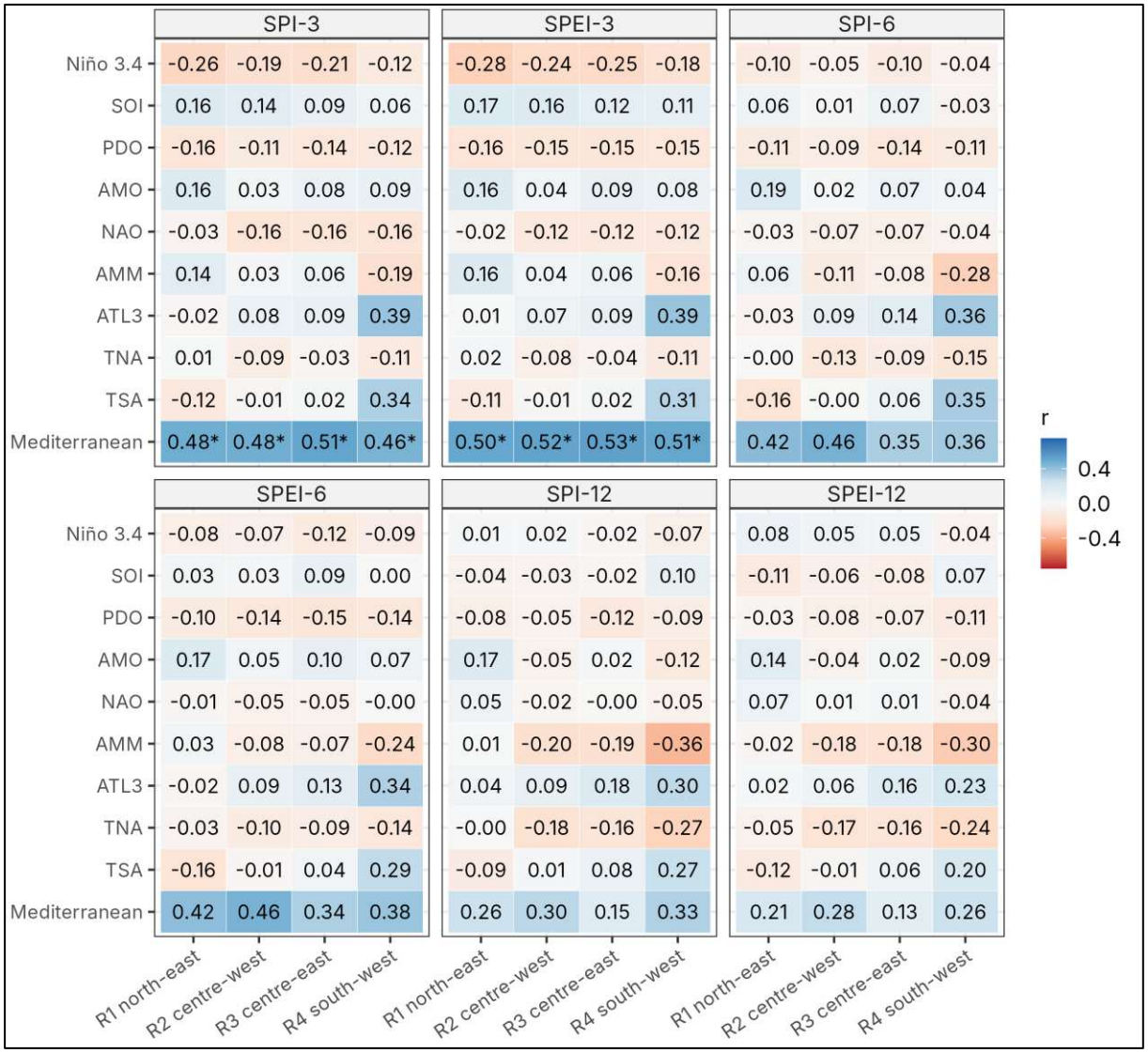


Fig. 8 Correlation between the SPI and SPEI of the regions and the ocean indices (1981–2025). Detrended series; ocean indices averaged over the same months as the drought index. ∗: significant after false discovery rate control. Sources: CHIRPS v2.0; AgERA5; NOAA PSL; ERSSTv5.

The composites confirm this result (Fig. 9). The Mediterranean is colder during dry years, which correspond to the lower tertile of each index – than during wet years, with a significant difference across all four regions for SPI-3 (from −0.89 to −1.11 standard deviations) and SPEI-3 (from −1.06 to −1.14). The difference remains significant at 6 months in the central-west (−0.85 for both indices) and in the south-west (−0.94 for the SPI-6), as well as at 12 months in the south-west (−0.77 for the SPI-12). A warmer Niño 3.4 is also associated with dry years on a quarterly scale (from +0.38 to +0.78

standard deviations), although the difference did not reach the significance threshold in any region ($p \geq 0.055$).

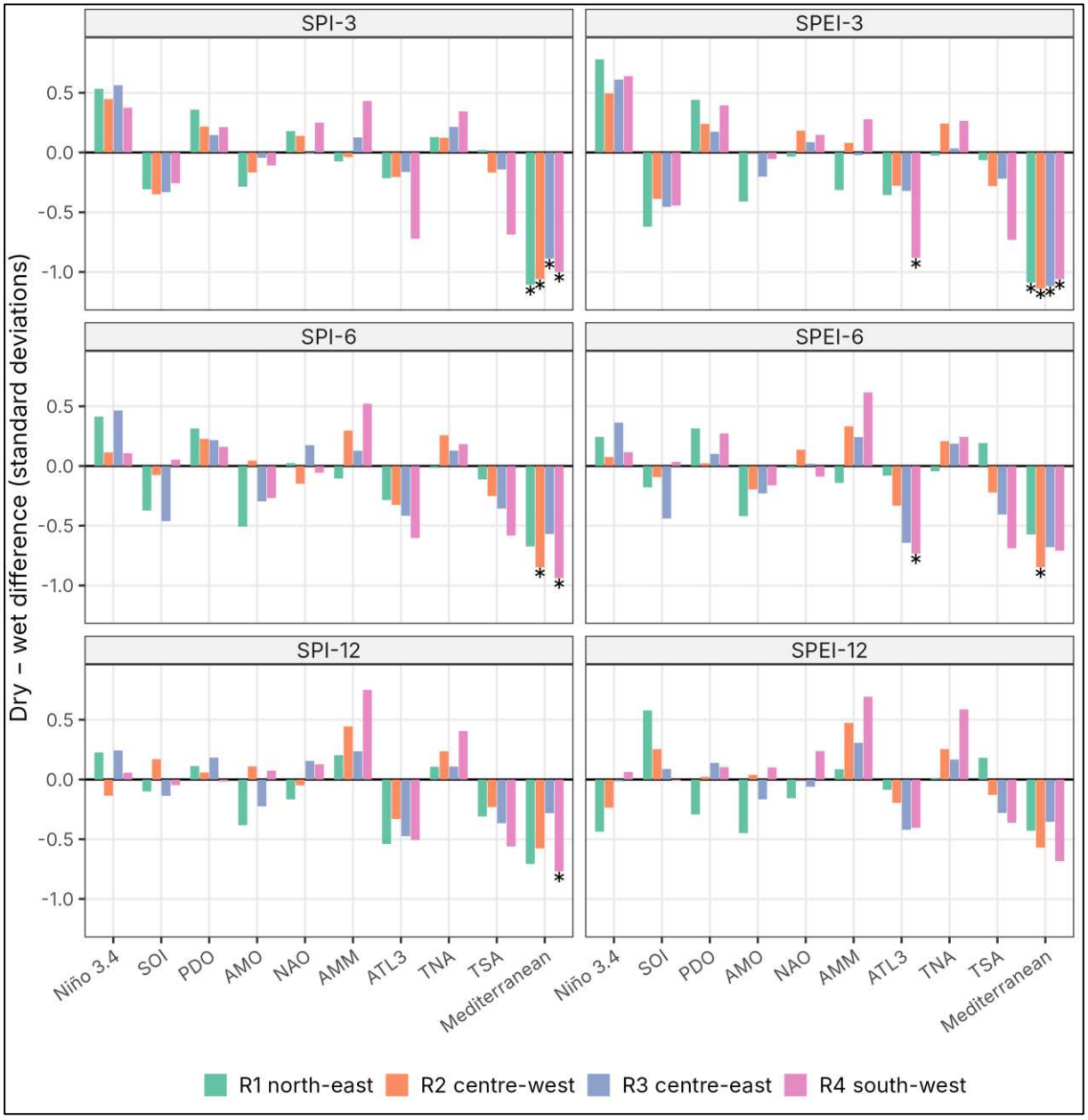


Fig. 9 Ocean indices during dry and wet years, for the six indices. Difference between the mean of dry years (lower tercile) and that of wet years (upper tercile), in standard deviations; ocean indices averaged over the same months as the drought index. ∗: $p < 0.05$ (permutation test). Sources: CHIRPS v2.0; AgERA5; NOAA PSL; ERSSTv5.

3.3.2 The Gulf of Guinea in the south-west, ENSO until the mid-2000s

A second link, with the Gulf of Guinea, highlights the south-west, where the six indices show a positive correlation with ATL3, ranging from +0.39 (SPI-3 and SPEI-3) to +0.23 (SPEI-12), as well as with the tropical South Atlantic (+0.20 to +0.35); in the other three regions, these correlations do not exceed +0.18. This link is independent of ENSO: the ATL3 and Niño 3.4 from July to September show a correlation of only −0.31, and, once Niño 3.4 is excluded, the partial correlation of the ATL3 with the 3- and 6-month indices

for the south-west remains between +0.33 and +0.37. Dry years in the south-west are accompanied by a cooling of the Gulf of Guinea of 0.88 standard deviations for the SPEI-3 (p = 0.02) and 0.73 for the SPEI-6 (p = 0.04); the difference, which has the same sign as that observed with the SPI, is, however, on the borderline of significance (−0.72 for the SPI-3, p = 0.054). This relationship proves to be stable on a 3-month timescale. Over 15-year moving windows, the correlation for the south-west remains positive throughout the period (+0.17 to +0.73 depending on the index), whilst that for the other regions, on the same timescale, becomes negative for windows centred after 2013 (−0.17 to −0.38; Fig. 10).

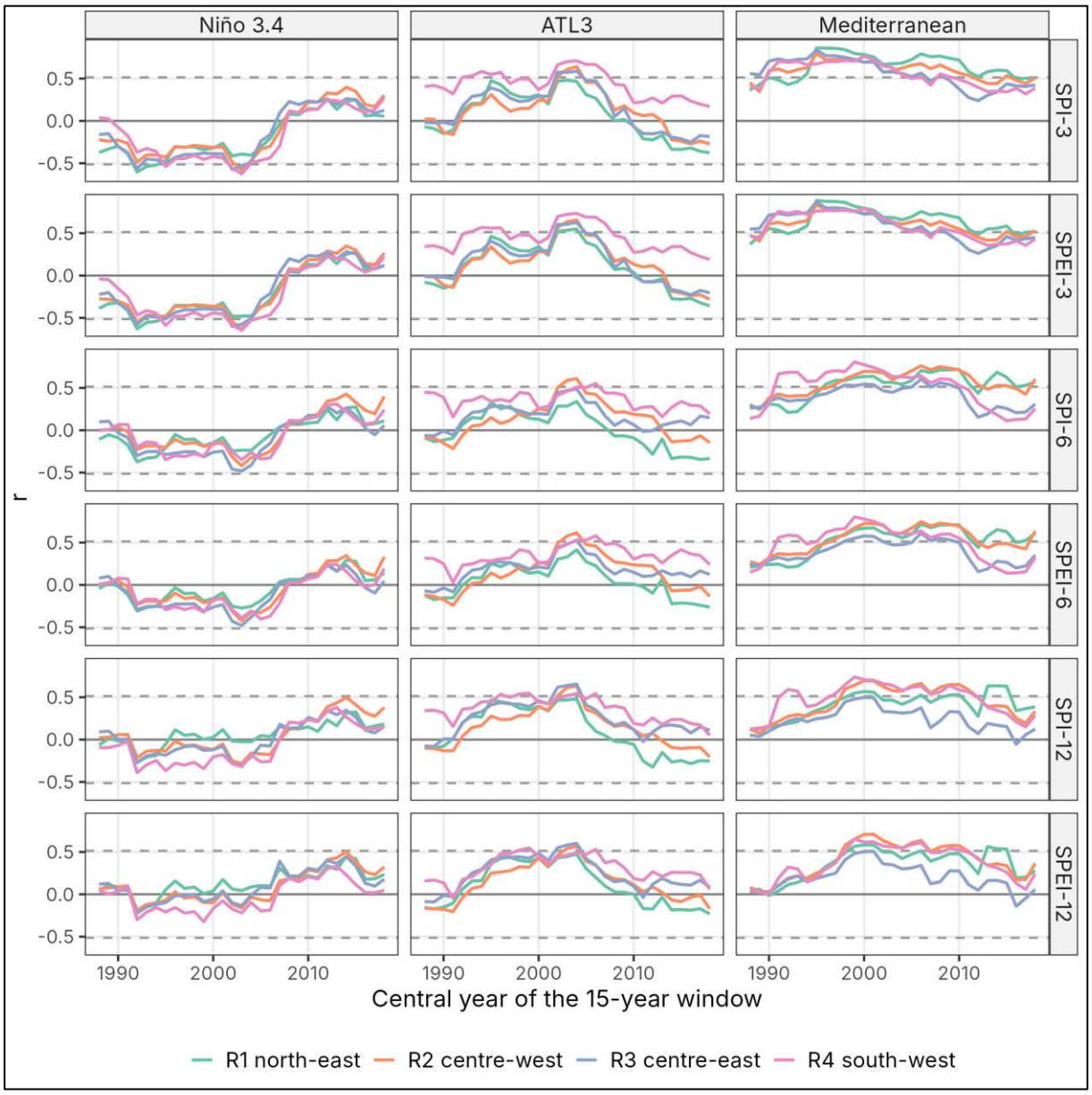


Fig. 10 Rolling correlations (15-year windows) between the SPI and SPEI of the regions and three ocean indices. x-axis: central year of the window; dashes: 5% significance threshold. Sources: CHIRPS v2.0; AgERA5; NOAA PSL; ERSSTv5.

The other correlations evolve over time in the same way for all six indices (Figs. 10 and 11). The correlation with ENSO is strongest at the 3-month timescale: negative or zero in all regions up to the windows centred on 2006, reaching −0.63 for the SPI-3 and −0.65 for the SPEI-3 in the 1996–2010 window, whilst it is weaker and more irregular at 6 months (maximum −0.48) and at 12 months (maximum between −0.32 and −0.39). From the windows centred on 2008 onwards, it disappears for all indices (ranging from −0.09 to +0.50), and the correlation even becomes positive between 2011 and 2020, across all regions and for all indices (ranging from +0.09 to +0.63). This positive value is, however, partly due to the year 2015. Once this is excluded, the three-month correlation remains between +0.43 and +0.46 in the centre-west and south-west, but falls to between −0.02 and +0.13 in the north-east and centre-east; over the period 2011–2025, it is close to zero in all four regions (between −0.16 and −0.01). The weakening of this link is therefore well established, but not its reversal. In the north and centre, by contrast, the correlation was negative between 1981 and 1990 for all six indices (ranging from −0.17 to −0.67). The link with the Mediterranean reached its peak between 1991 and 2000 on a quarterly basis (+0.64 to +0.91), and its decadal variations are more moderate over 6- and 12-month periods. Calculated using ten values, these ten-year correlations are fragile when considered in isolation, but their overall trend remains consistent across regions and indices.

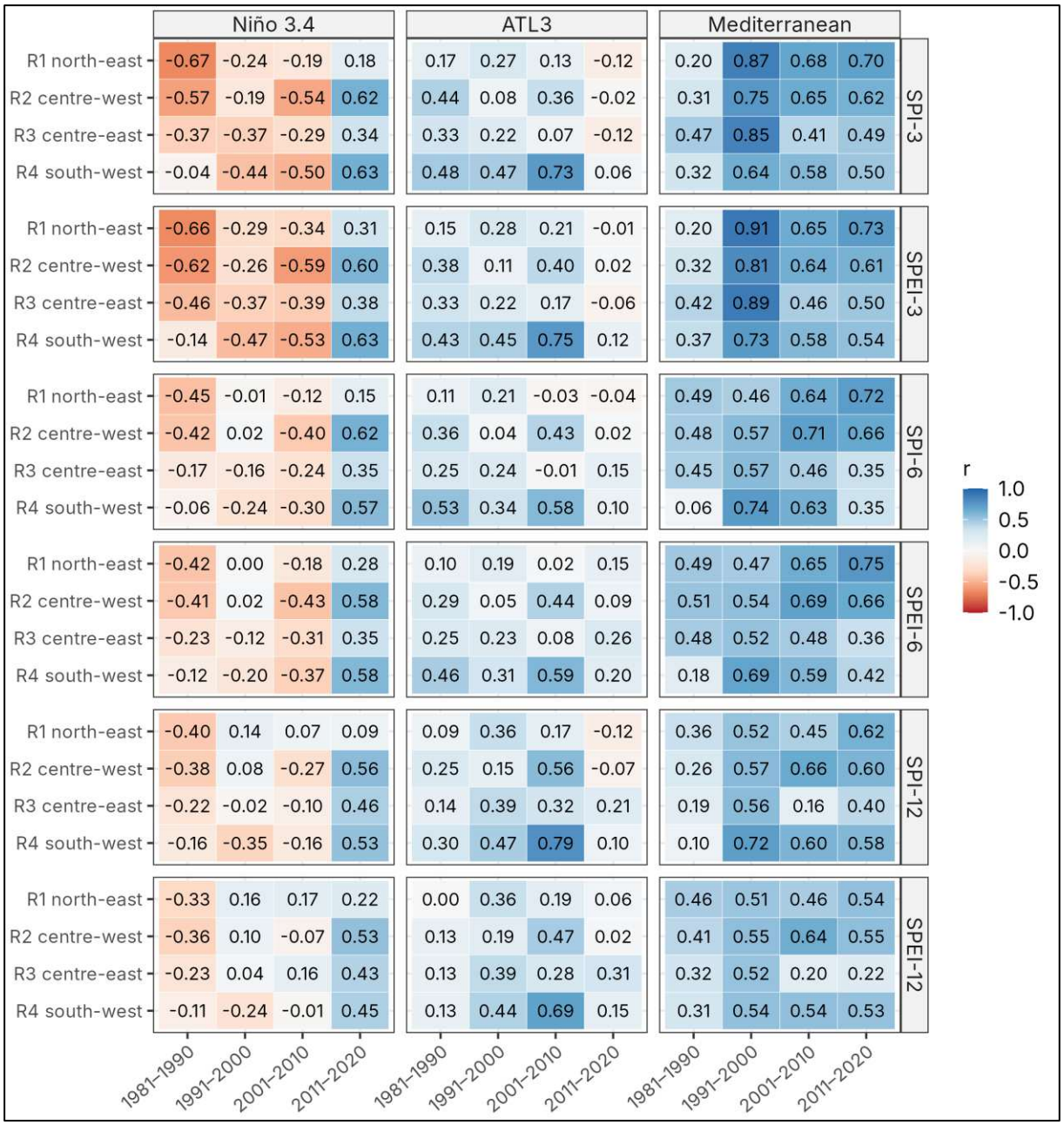


Fig. 11 Correlation by decade between the SPI and SPEI of the regions and three ocean indices. Detrended series; ten values per decade. Sources: CHIRPS v2.0; AgERA5; NOAA PSL; ERSSTv5.

Wavelet coherence analysis makes it possible to identify the timescales over which these links operate (Fig. 12; whole period by band: Fig. 13). Over the entire period and in the 2–7-year band, the ATL3 is, with a few exceptions, the oceanic index showing the strongest coherence with drought in the north-east, centre-west and centre-east (ranging from 12 to 39 per cent of significant cells depending on the index). The exceptions concern the SPI-3, which shows slightly stronger consistency with the AMO (24–25 per cent), and the SPEI-3 in the central-west, which shows slightly stronger consistency with the Mediterranean. In the south-west, no single oceanic index stands out (10–20 per cent for the ATL3, the PDO and the Mediterranean). Virtually absent until 2010 for all six indices (0–14 per cent), consistency with ENSO emerged between 2011 and 2020, at the very moment when the correlation began to fade. There is no contradiction here: as it is insensitive to the sign of the relationship, the consistency in

this case reveals a link whose phase has changed. It mainly concerns the SPI and SPEI-12 in the north and centre (15–51 per cent) and remains weak for SPEI-3 and SPEI-6 (1–15 per cent) as well as in the south-west (0–8 per cent). Consistency with the PDO, which was pronounced between 1981 and 1990 – particularly in the south-west, where it covered 40–67 per cent of cells depending on the index – weakened significantly thereafter; correlation with the AMO is notable in 2011–2020 in the central-west and central-east for the 6- and 12-month indices (34–68 per cent for the SPI-6, SPI-12 and SPEI-12). In the 8–16-year band (Fig. 13), consistency is concentrated in the south-west, where the NAO occupies up to 93 per cent of the cells and the Mediterranean and ATL3 up to 70 and 67 per cent, respectively, as well as in the central-west with ATL3 (up to 69 per cent). Over a 45-year period, however, this band contains only three to five cycles, which means these values must be interpreted with caution.

Table 5 summarises these relationships for each region.

Table 5 Summary of the teleconnections associated with the drought of each region, for the six indices

Region	Stable link (1981–2025)	Links changing over time	Wavelet coherence (2–7 years)
R1 north-east	Mediterranean: r = +0.48 (SPI-3) and +0.50 (SPEI-3); dry years −1.11 and −1.09 SD	ENSO negative until the mid-2000s (−0.66 and −0.67 at 3 months in 1981–1990), then nil (+0.31 in 2011–2020, +0.13 without 2015)	ATL3 (16 to 39% depending on the index), increasing over the decades for the SPEI-12 (22 to 48%)
R2 centre-west	Mediterranean: +0.48 and +0.52; −1.06 and −1.14 SD (also at 6 months: −0.85)	ENSO negative until the mid-2000s, then positive but fragile (+0.62 in 2011–2020, +0.44 without 2015)	ATL3 (12 to 32%); in 2011–2020, ENSO (up to 51%) and AMO (up to 56%), mainly at the 6- and 12-month scales
R3 centre-east	Mediterranean: +0.51 and +0.53; −0.89 and −1.12 SD	ENSO negative until the mid-2000s, then nil (+0.38 in 2011–2020, +0.12 without 2015)	ATL3 (16 to 32%); AMO in 2011–2020 (41 to 68% for the SPI-6, SPI-12 and SPEI-12)
R4 south-west	Mediterranean: +0.46 and +0.51; −1.00 and −1.06 SD; Gulf of Guinea: ATL3 +0.23 to +0.39 (significant composites with the SPEI-3 and SPEI-6)	ENSO negative from 1991 to 2010 at 3-month scales (−0.44 to −0.53), then positive but fragile (+0.63 in 2011–2020, +0.46 without 2015)	no dominant index (10 to 20%); PDO in 1981–1990 (40 to 67%); at 8–16 years: NAO and ATL3

r: correlation with the 3-month index (SPI-3, then SPEI-3); SD: difference between dry and wet years, in standard deviations. Percentages: share of significant cells outside the cone of influence, depending on the drought index.

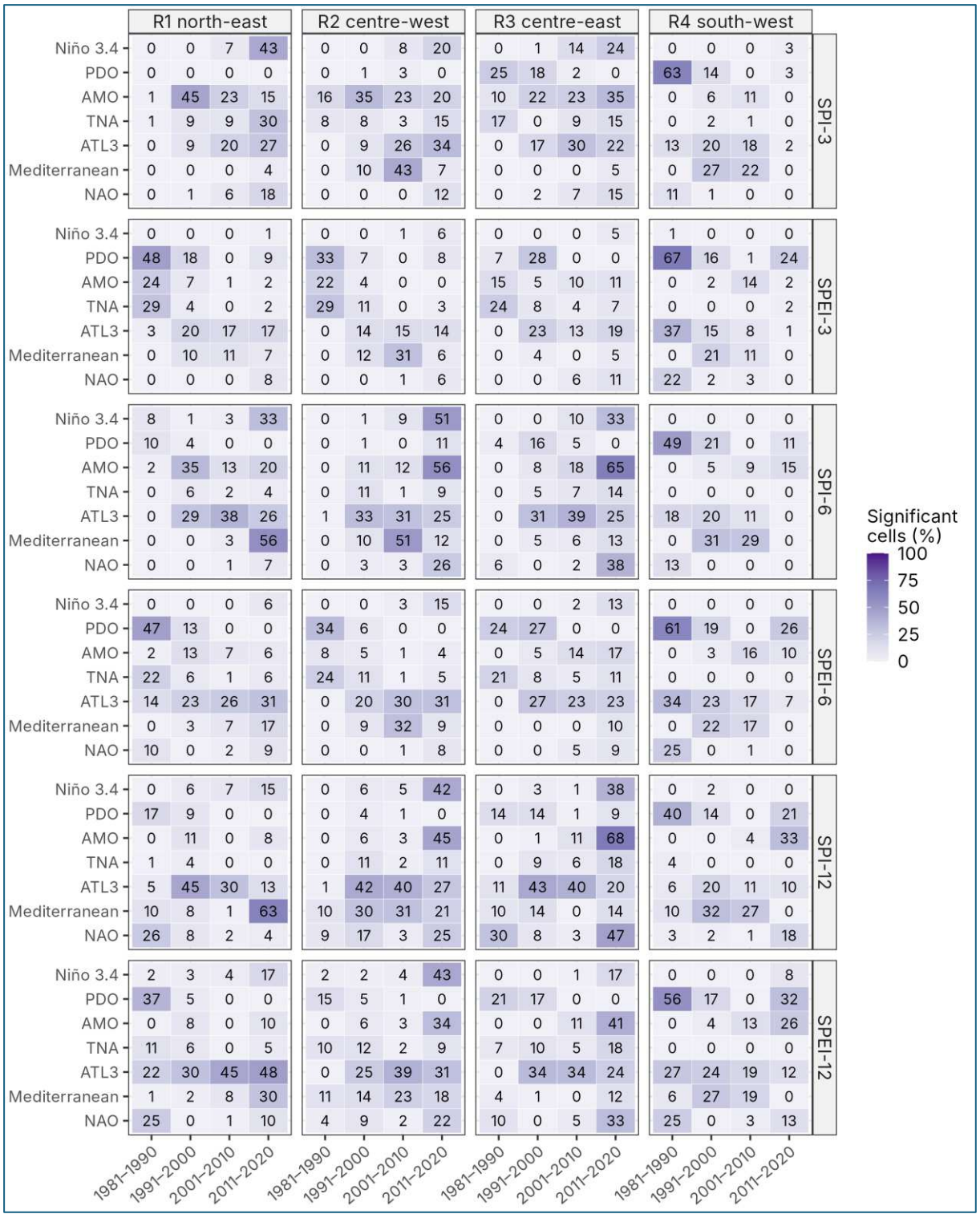


Fig. 12 Wavelet coherence (2–7-year band) between the SPI and SPEI of the regions and the ocean indices, by decade. Share of cells significant at 95% (200 red-noise simulations) outside the cone of influence. Grey: fewer than 100 cells. Sources: CHIRPS v2.0; AgERA5; NOAA PSL; ERSSTv5.

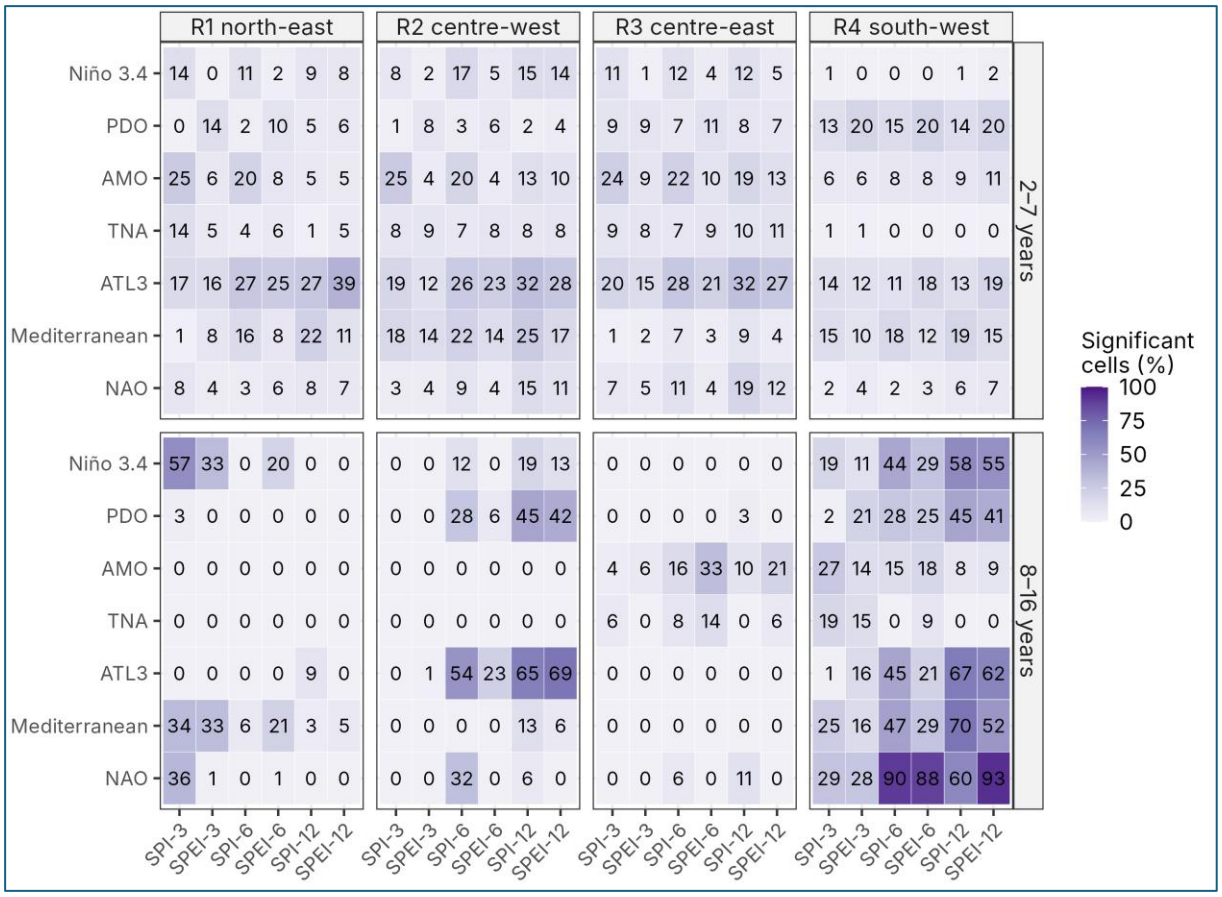


Fig. 13 Wavelet coherence over the whole period (1981–2025), by period band, between the SPI and SPEI of the regions and the ocean indices. Share of cells significant at 95% (200 red-noise simulations) outside the cone of influence. Sources: CHIRPS v2.0; AgERA5; NOAA PSL; ERSSTv5.

4 Discussion

4.1 Delineating homogeneous drought regions

Rather than simply reflecting a latitudinal stratification, the four regions thus defined also highlight, in the centre of the country, a contrast between the east and the west. This dual structure is consistent with the spatial pattern of African rainfall anomalies, which are pronounced along latitudinal bands but interrupted by zonal discontinuities [51], as well as with West African drought regimes, which separate the eastern Sahel from the western Sahel [15]. The north-east of Burkina Faso, where drought has receded the most, forms part of the central Sahel, where the recovery in rainfall has been most pronounced [1, 3, 52]. The south-west, meanwhile, belongs to the Sudanese domain, where rainfall patterns have not followed the same trend as those of the Sahel since the 1970s [53, 54]. Far from being a mere statistical artefact, the drought region thus corresponds to distinct climatic regimes.

The fact that the south-west remains stable regardless of the index used, and that the boundaries of the centre-east are fragile, is consistent with the results of regionalisation studies conducted elsewhere, in which the most contrasting regions always emerge,

whilst transition zones shift from one group to another depending on the index and timescale [12–14]. With a silhouette of 0.36, the SPEI-12 partition also belongs to the category of weak structures as defined by Rousseeuw [44]; the regions are real but their boundaries are imprecise, a situation that frequently arises when varimax rotation distributes contact provinces between two components [11]. The differences between the indices also have a physical explanation. As evaporative demand is spatially more homogeneous than precipitation, the 3-month SPEI groups together provinces with disparate precipitation patterns, whilst the seasonal SPI distinguishes the far east, where precipitation from July to October evolves partly independently of the rest of the country. The characteristics of the rainy season (start, end and duration) also vary considerably from one region to another [55, 56]. There is therefore no single regionalisation; each depends on the type of drought to be monitored: small-scale agricultural drought or large-scale hydrological drought [19].

The 2025 administrative division covers these regions only partially (Table 2). Whilst the south-west, which corresponds exactly to three administrative regions, lends itself easily to joint monitoring, Koulsé and Nando straddle two regions affected by drought, meaning that their provinces do not experience drought in the same years and that a regional average would mask differing situations. However, the national forecasting and warning system publishes its bulletins at the level of administrative regions, based on deviation from the norm and the SPI index, without using the SPEI index [57], whilst the national meteorological service's monitoring is carried out by climatic zones and isohyets [58]. More homogeneous than administrative regions and more detailed than climate zones, drought regions provide an intermediate framework that could serve as a reference grid for agrometeorological bulletins and the early warning system. This conclusion depends, however, partly on the method used, as a different classification criterion might reclassify certain provinces from the central zone, without, however, calling into question the two poles.

4.2 Characterizing decadal drought variability and the share of evaporative demand

The general chronology of the Sahel can be observed: a very dry decade (1981–1990) was followed, from the 1990s onwards, by a recovery in rainfall [1–3, 59]. In Burkina Faso, this recovery has already been documented using cumulative rainfall data, seasonal descriptors and anomaly indices [6, 7, 9, 56]. A regional analysis shows that this recovery has not been of the same magnitude everywhere. In the north and centre, the six indices show increases ranging from 1.09 to 1.82 standard deviations, and each of these increases is statistically significant, whereas none are significant in the south-west. Furthermore, this recovery is accompanied by more intense and erratic rainfall [4, 5] and, in the Sahel, by a paradoxical increase in runoff despite cumulative totals

that remain lower than those prior to 1970 [54, 60]; the decline in meteorological drought therefore does not necessarily imply a decline in hydrological drought.

The uniqueness of the south-west is the most striking finding of this study. Although it is the country's wettest region, it is the only one where drought has not decreased significantly since the 1980s, and it was during the period 2001–2010 that the highest number of drought episodes occurred there, as measured by the SPEI-6 and SPEI-12 indices. Two mechanisms contribute to this situation. The first relates to rainfall: the recovery in rainfall has mainly benefited the central Sahel [1, 2], whilst rainfall in the south-west is more strongly influenced by the Gulf of Guinea, whose variability differs from that of the Sahel [53]. According to the permutation test, the SPI, based solely on rainfall, does not increase significantly in this region, regardless of the scale considered, and its increases remain insignificant in the far south-west (+0.07 to +0.59), where rainfall has not recovered. The second mechanism concerns evaporation demand, the role of which is a matter of debate: estimates based solely on temperature overestimate the drying effect [61, 62], as wind, humidity and radiation are equally important factors [63–65]. Using the Penman-Monteith ET_0, the proportion of the SPI gain absorbed by evaporation demand increases here with the time scale, rising from 18 per cent over 3 months to 44 per cent over 12 months in the south-west, compared with 12 to 20 per cent in the other regions. This also supports studies that attribute part of the recent Sahelian drought to global warming [66, 67], whilst clarifying its extent: in Burkina Faso, this effect mainly affects the annual drought in the south-west, on which reservoir filling and aquifer recharge depend, and has little impact on seasonal drought.

This persistence has practical implications. The south-west, which accounts for 22 per cent of the country's territory and 78 local authorities, contributes a significant proportion of national cotton and cereal production; the impression that the drought is abating – whilst certainly accurate at national level – is therefore misleading in this region. Given that the SPI index, on its own, underestimates drought in this region, it would be useful, for monitoring purposes, to combine the SPI and SPEI indices, particularly over a 12-month period. It is still too early to draw conclusions from the 2021–2025 period, which was wet throughout the region, as five years do not constitute a decade; the dry years of 2021 and 2023 in the north-east warrant close monitoring, particularly as regional projections forecast shorter seasons and more irregular rainfall for Burkina Faso [59, 68]. Finally, as the distributions are fitted to the 1981–2025 period, decades are compared with one another rather than against an external normal; this approach is suitable for studying variability but not for declaring a state of drought, which requires a fixed reference period [18].

4.3 Identifying the teleconnections of each region and their stability over time

The link between the Mediterranean and drought during the rainy season is the strongest of those identified by this study. It may seem surprising that a sea situated more than 2,000 km north of Burkina Faso should have an impact on rainfall in that country, but the mechanism is well understood: it is a local teleconnection, based on the transport of moisture, and not, as in the case of ENSO, a remote influence transmitted by atmospheric waves. Rowell's [20] modelling experiments have shown that a warm eastern Mediterranean increases evaporation and that the air thus moistened moves southwards across the Sahara, carried by low-level north-easterly winds that blow in summer between the Saharan heat low and the Libyan high. On reaching the Sahel, this moistened air strengthens moisture convergence and convection along the intertropical convergence zone. The same relationship appears in the 1979–2006 observations of Fontaine et al. [21], in which warm Mediterranean summers are wetter over the Sahel and the rainband is displaced northwards. Simulations by Gaetani et al. [69] further indicate that the warming of the Mediterranean deepens the Saharan heat trough and weakens the East African jet stream, two conditions favourable to Sahelian precipitation. Finally, Park et al. [70] attribute part of the recovery in rainfall observed since the 1990s to this anthropogenic warming, to the extent that they regard it as a determining factor for future rainfall. The Mediterranean is therefore among the most stable statistical predictors of the monsoon [22, 71]. The positive sign of the link, its maximum at the 3-month scale and its homogeneity across the four regions all match this mechanism, which acts over the whole monsoon belt. Because it is computed on detrended series, the link reflects shared interannual variability rather than the coincidence of sea warming and rainfall recovery. Two features are specific to Burkina Faso. The link reaches the Sudanian south-west, and it is almost identical for the SPI and the SPEI, which shows that it operates through rainfall rather than through evaporative demand. At the 3-month scale, however, it weakens after its 1991–2000 maximum, so that the Mediterranean should not be treated as a sole predictor.

The dipole structure of the Gulf of Guinea's response explains the positive link between ATL3 and drought in the south-west. When the Gulf is warm, the rainy zone shifts southwards, increasing rainfall along the Guinean coast and reducing it in the Sahel [24, 25, 72, 73]. Between 9.5° and 12° N, south-western Burkina Faso lies within the southern branch of this dipole, where a warm Gulf continues to favour rainfall, whilst the north and centre occupy the transition zone, where the two effects cancel each other out. Two reservations nevertheless apply. First, Losada et al. [23] found that this dipole is no longer observed after the 1970s and that the equatorial Atlantic now covaries with ENSO, so that part of the signal attributed to the ATL3 could be common

to the two basins. That is not the case here: once Niño 3.4 is removed, the partial correlation between the ATL3 and south-western drought remains between +0.33 and +0.37, which points to an effect specific to the Gulf of Guinea. Second, the correlations over the whole period (+0.23 to +0.39) do not survive the correction for multiple tests, and only the SPEI-3 and SPEI-6 composites are significant; the Gulf of Guinea would then also act on evaporative demand, through cloudiness and air humidity, a hypothesis that remains to be tested.

The disappearance of the link with ENSO after the mid-2000s illustrates the widely documented non-stationarity of the relationship between ENSO and the Sahel [23, 74–77]. This relationship is determined by the background state of the Atlantic and Pacific, modulated by the PDO and the AMO [78, 79]; the coherence of wavelets with the PDO in the 1980s, and subsequently with the AMO in the 2010s, supports this view. In Burkina Faso, this attenuation, which occurred in the mid-2000s, thus extends to drought in all regions and for all six indices. It would nevertheless be an exaggeration to speak of a reversal, as the positive correlation for 2011–2020 is based on only ten years and disappears over the 2011–2025 period once the 2015 El Niño is excluded. Decadal correlations and moving windows are only meaningful when considered in terms of their overall trend. As for the wavelet analysis, which has shown elsewhere how the influence of oscillations varies from one timescale to another [80], it is based on Monte Carlo simulations, the order of which alters the proportion of significant cells by less than 2 points in 90 per cent of cases. This has two implications for seasonal forecasts. The Mediterranean should be included amongst the predictors of drought during the rainy season across the whole country, alongside the Pacific and Atlantic indices usually considered; furthermore, predictors should be selected on a region-by-region basis and reassessed over time, as a link that was relevant in the 1990s may no longer be useful today.

5 Conclusion

Based on the 3-, 6- and 12-month SPI and SPEI indices calculated for the 47 provinces, this study examined the spatial and decadal variability of drought in Burkina Faso from 1981 to 2025, as well as the associated teleconnections. Three main findings emerge.

Firstly, drought is organised into four homogeneous regions: the north-eastern Sahel, the central-west, the central-east and the south-western Sudan region, the boundaries of which do not correspond to the administrative divisions of 2025. Whilst the south-west remains stable regardless of the index, and the north-east almost as stable, the internal boundaries of the central part of the country vary depending on the index and the scale.

Secondly, although the decade 1981–1990 was, on average, the driest everywhere and for all six indices, drought has since then only significantly decreased in the north and centre. In the south-west, it re-emerged between 2001 and 2010 and persisted until 2020, with evaporation demand there absorbing a larger share of the increase in precipitation than elsewhere, rising from 18 per cent over 3 months to 44 per cent over 12 months.

Thirdly, Mediterranean temperature is the only factor common to all regions and significant over the entire period, for both SPI-3 and SPEI-3. The Gulf of Guinea plays a role mainly in the south-west, independently of ENSO, whose link with drought – evident until the mid-2000s – has since weakened without reversing permanently. Drought monitoring and forecasting in Burkina Faso would therefore benefit from being carried out on a drought-region basis, using an index that takes into account evaporation demand and oceanic predictors specific to each region, which are regularly reassessed.

Declarations

Acknowledgments. The authors thank CHIRPS, AgERA5, NOAA PSL, ERSSTv5, OCHA for the data.

Funding: This research did not receive any funding.

Authors contributions: Joseph Yaméogo: Research ideas, Conceptualization, Data acquisition, Statistical analysis of data, Methodology, Manuscript writing; Songanaba ROUAMBA: Statistical analysis of data, Methodology, Manuscript writing.

Data availability statements: All datasets used are publicly available (CHIRPS, AgERA5, NOAA PSL, ERSSTv5, OCHA).

Ethics approval: Not applicable

Consent to participate: Not applicable.

Consent for publication: Not applicable.

Clinical trial: Not applicable

Competing interests: The authors declare no competing interests

References

1. Lebel T, Ali A. Recent trends in the Central and Western Sahel rainfall regime (1990–2007). Journal of Hydrology. 2009;375(1–2):52–64. https://doi.org/10.1016/j.jhydrol.2008.11.030
2. Sanogo S, Fink AH, Omotosho JA, Ba A, Redl R, Ermert V. Spatio-temporal characteristics of the recent rainfall recovery in West Africa. International Journal of Climatology. 2015;35(15):4589–4605. https://doi.org/10.1002/joc.4309
3. Nicholson SE, Fink AH, Funk C. Assessing recovery and change in West Africa's rainfall regime from a 161-year record. International Journal of Climatology. 2018;38(10):3770–3786. https://doi.org/10.1002/joc.5530

4. Panthou G, Vischel T, Lebel T. Recent trends in the regime of extreme rainfall in the Central Sahel. International Journal of Climatology. 2014;34(15):3998–4006. https://doi.org/10.1002/joc.3984
5. Taylor CM, Belušić D, Guichard F, et al.. Frequency of extreme Sahelian storms tripled since 1982 in satellite observations. Nature. 2017;544(7651):475–478. https://doi.org/10.1038/nature22069
6. De Longueville F, Hountondji Y-CH, Kindo I, Gemenne F, Ozer P. Long-term analysis of rainfall and temperature data in Burkina Faso (1950–2013). International Journal of Climatology. 2016;36(13):4393–4405. https://doi.org/10.1002/joc.4640
7. Yanogo IP, Yaméogo J. Recent rainfall trends between 1990 and 2020: contrasting characteristics between two climate zones in Burkina Faso (West Africa). Glasnik Srpskog geografskog društva / Bulletin of the Serbian Geographical Society. 2023;103(1):87–106. https://doi.org/10.2298/GSGD2301087Y
8. Yaméogo J, Koala S, Rouamba S, Yanogo IP. Spatial distribution and temporal trends in precipitation concentration indices over Burkina Faso from 1993 to 2023. Discover Environment. 2026;4:54. https://doi.org/10.1007/s44274-026-00564-z
9. Yaméogo J, Rouamba S, Koala S. Meteorological drought trends in Burkina Faso (1991–2023): a monthly and seasonal rainfall anomaly index analysis. AUC Geographica. 2026. Online ahead of print. https://doi.org/10.14712/23361980.2026.13
10. Yaméogo J, Yo B, Zorom A, Yanogo IP. Spatio-temporal analysis of extreme rainfall indices in Burkina Faso using RClimDex. African Geographical Review. 2026. Online ahead of print. https://doi.org/10.1080/19376812.2026.2689349
11. Richman MB. Rotation of principal components. Journal of Climatology. 1986;6(3):293–335. https://doi.org/10.1002/joc.3370060305
12. Vicente-Serrano SM. Spatial and temporal analysis of droughts in the Iberian Peninsula (1910–2000). Hydrological Sciences Journal. 2006;51(1):83–97. https://doi.org/10.1623/hysj.51.1.83
13. Raziei T, Saghafian B, Paulo AA, Pereira LS, Bordi I. Spatial patterns and temporal variability of drought in western Iran. Water Resources Management. 2009;23(3):439–455. https://doi.org/10.1007/s11269-008-9282-4
14. Santos JF, Pulido-Calvo I, Portela MM. Spatial and temporal variability of droughts in Portugal. Water Resources Research. 2010;46(3):W03503. https://doi.org/10.1029/2009WR008071
15. Diasso U, Abiodun BJ. Drought modes in West Africa and how well CORDEX RCMs simulate them. Theoretical and Applied Climatology. 2017;128(1–2):223–240. https://doi.org/10.1007/s00704-015-1705-6
16. McKee TB, Doesken NJ, Kleist J. The relationship of drought frequency and duration to time scales. In: Proceedings of the 8th Conference on Applied Climatology. Anaheim: American Meteorological Society; 1993. p. 179–184.
17. Vicente-Serrano SM, Beguería S, López-Moreno JI. A multiscalar drought index sensitive to global warming: the Standardized Precipitation Evapotranspiration Index. Journal of Climate. 2010;23(7):1696–1718. https://doi.org/10.1175/2009JCLI2909.1
18. Wilhite DA, Glantz MH. Understanding the drought phenomenon: the role of definitions. Water International. 1985;10(3):111–120. https://doi.org/10.1080/02508068508686328
19. Mishra AK, Singh VP. A review of drought concepts. Journal of Hydrology. 2010;391(1–2):202–216. https://doi.org/10.1016/j.jhydrol.2010.07.012
20. Rowell DP. The impact of Mediterranean SSTs on the Sahelian rainfall season. Journal of Climate. 2003;16(5):849–862. https://doi.org/10.1175/1520-0442(2003)016<0849:TIOMSO>2.0.CO;2
21. Fontaine B, Garcia-Serrano J, Roucou P, et al.. Impacts of warm and cold situations in the Mediterranean basins on the West African monsoon: observed connection patterns (1979–2006) and climate simulations. Climate Dynamics. 2010;35(1):95–114. https://doi.org/10.1007/s00382-009-0599-3
22. Rodríguez-Fonseca B, Mohino E, Mechoso CR, et al.. Variability and predictability of West African droughts: a review on the role of sea surface temperature anomalies. Journal of Climate. 2015;28(10):4034–4060. https://doi.org/10.1175/JCLI-D-14-00130.1
23. Losada T, Rodríguez-Fonseca B, Mohino E, Bader J, Janicot S, Mechoso CR. Tropical SST and Sahel rainfall: a non-stationary relationship. Geophysical Research Letters. 2012;39(12):L12705. https://doi.org/10.1029/2012GL052423
24. Polo I, Rodríguez-Fonseca B, Losada T, García-Serrano J. Tropical Atlantic variability modes (1979–2002). Part I: time-evolving SST modes related to West African rainfall. Journal of Climate. 2008;21(24):6457–6475. https://doi.org/10.1175/2008JCLI2607.1
25. Nnamchi HC, Li J. Influence of the South Atlantic Ocean dipole on West African summer precipitation. Journal of Climate. 2011;24(4):1184–1197. https://doi.org/10.1175/2010JCLI3668.1
26. Funk C, Peterson P, Landsfeld M, et al.. The climate hazards infrared precipitation with stations—a new environmental record for monitoring extremes. Scientific Data. 2015;2:150066. https://doi.org/10.1038/sdata.2015.66
27. OCHA. Burkina Faso – Subnational administrative boundaries (admin 0 to 3, version 3, valid as of 1 August 2025). United Nations Office for the Coordination of Humanitarian Affairs, Humanitarian Data Exchange; 2025.
28. Dembélé M, Zwart SJ. Evaluation and comparison of satellite-based rainfall products in Burkina Faso, West Africa. International Journal of Remote Sensing. 2016;37(17):3995–4014. https://doi.org/10.1080/01431161.2016.1207258
29. C3S. Agrometeorological indicators from 1979 to present derived from reanalysis. Copernicus Climate Change Service, Climate Data Store; 2020. https://doi.org/10.24381/cds.6c68c9bb
30. Allen RG, Pereira LS, Raes D, Smith M. Crop evapotranspiration: guidelines for computing crop water requirements. FAO Irrigation and Drainage Paper 56. Rome: FAO; 1998.
31. Trenberth KE. The definition of El Niño. Bulletin of the American Meteorological Society. 1997;78(12):2771–2777. https://doi.org/10.1175/1520-0477(1997)078<2771:TDOENO>2.0.CO;2
32. Mantua NJ, Hare SR, Zhang Y, Wallace JM, Francis RC. A Pacific interdecadal climate oscillation with impacts on salmon production. Bulletin of the American Meteorological Society. 1997;78(6):1069–1079. https://doi.org/10.1175/1520-0477(1997)078<1069:APICOW>2.0.CO;2

33. Enfield DB, Mestas-Nuñez AM, Trimble PJ. The Atlantic multidecadal oscillation and its relation to rainfall and river flows in the continental U.S.. Geophysical Research Letters. 2001;28(10):2077–2080. https://doi.org/10.1029/2000GL012745
34. Hurrell JW. Decadal trends in the North Atlantic Oscillation: regional temperatures and precipitation. Science. 1995;269(5224):676–679. https://doi.org/10.1126/science.269.5224.676
35. Enfield DB, Mestas-Nuñez AM, Mayer DA, Cid-Serrano L. How ubiquitous is the dipole relationship in tropical Atlantic sea surface temperatures? Journal of Geophysical Research: Oceans. 1999;104(C4):7841–7848. https://doi.org/10.1029/1998JC900109
36. Chiang JCH, Vimont DJ. Analogous Pacific and Atlantic meridional modes of tropical atmosphere–ocean variability. Journal of Climate. 2004;17(21):4143–4158. https://doi.org/10.1175/JCLI4953.1
37. Zebiak SE. Air–sea interaction in the equatorial Atlantic region. Journal of Climate. 1993;6(8):1567–1586. https://doi.org/10.1175/1520-0442(1993)006<1567:AIITEA>2.0.CO;2
38. Huang B, Thorne PW, Banzon VF, et al.. Extended Reconstructed Sea Surface Temperature, Version 5 (ERSSTv5): upgrades, validations, and intercomparisons. Journal of Climate. 2017;30(20):8179–8205. https://doi.org/10.1175/JCLI-D-16-0836.1
39. Hosking JRM. L-moments: analysis and estimation of distributions using linear combinations of order statistics. Journal of the Royal Statistical Society: Series B. 1990;52(1):105–124. https://doi.org/10.1111/j.2517-6161.1990.tb01775.x
40. Beguería S, Vicente-Serrano SM, Reig F, Latorre B. Standardized precipitation evapotranspiration index (SPEI) revisited: parameter fitting, evapotranspiration models, tools, datasets and drought monitoring. International Journal of Climatology. 2014;34(10):3001–3023. https://doi.org/10.1002/joc.3887
41. Stagge JH, Tallaksen LM, Gudmundsson L, Van Loon AF, Stahl K. Candidate distributions for climatological drought indices (SPI and SPEI). International Journal of Climatology. 2015;35(13):4027–4040. https://doi.org/10.1002/joc.4267
42. Kaiser HF. The varimax criterion for analytic rotation in factor analysis. Psychometrika. 1958;23(3):187–200. https://doi.org/10.1007/BF02289233
43. Ward JH. Hierarchical grouping to optimize an objective function. Journal of the American Statistical Association. 1963;58(301):236–244. https://doi.org/10.1080/01621459.1963.10500845
44. Rousseeuw PJ. Silhouettes: a graphical aid to the interpretation and validation of cluster analysis. Journal of Computational and Applied Mathematics. 1987;20:53–65. https://doi.org/10.1016/0377-0427(87)90125-7
45. Hubert L, Arabie P. Comparing partitions. Journal of Classification. 1985;2(1):193–218. https://doi.org/10.1007/BF01908075
46. Yevjevich V. An objective approach to definitions and investigations of continental hydrologic droughts. Hydrology Papers 23. Fort Collins: Colorado State University; 1967.
47. Bretherton CS, Widmann M, Dymnikov VP, Wallace JM, Bladé I. The effective number of spatial degrees of freedom of a time-varying field. Journal of Climate. 1999;12(7):1990–2009. https://doi.org/10.1175/1520-0442(1999)012<1990:TENOSD>2.0.CO;2
48. Benjamini Y, Hochberg Y. Controlling the false discovery rate: a practical and powerful approach to multiple testing. Journal of the Royal Statistical Society: Series B. 1995;57(1):289–300. https://doi.org/10.1111/j.2517-6161.1995.tb02031.x
49. Grinsted A, Moore JC, Jevrejeva S. Application of the cross wavelet transform and wavelet coherence to geophysical time series. Nonlinear Processes in Geophysics. 2004;11(5/6):561–566. https://doi.org/10.5194/npg-11-561-2004
50. Torrence C, Compo GP. A practical guide to wavelet analysis. Bulletin of the American Meteorological Society. 1998;79(1):61–78. https://doi.org/10.1175/1520-0477(1998)079<0061:APGTWA>2.0.CO;2
51. Nicholson SE. The spatial coherence of African rainfall anomalies: interhemispheric teleconnections. Journal of Climate and Applied Meteorology. 1986;25(10):1365–1381. https://doi.org/10.1175/1520-0450(1986)025<1365:TSCOAR>2.0.CO;2
52. Ali A, Lebel T. The Sahelian standardized rainfall index revisited. International Journal of Climatology. 2009;29(12):1705–1714. https://doi.org/10.1002/joc.1832
53. Paturel J-E, Servat E, Kouamé B, Lubès H, Ouedraogo M, Masson J-M. Climatic variability in humid Africa along the Gulf of Guinea. Part II: an integrated regional approach. Journal of Hydrology. 1997;191(1–4):16–36.
54. Descroix L, Mahé G, Lebel T, et al.. Spatio-temporal variability of hydrological regimes around the boundaries between Sahelian and Sudanian areas of West Africa: a synthesis. Journal of Hydrology. 2009;375(1–2):90–102. https://doi.org/10.1016/j.jhydrol.2008.12.012
55. Ibrahim B, Polcher J, Karambiri H, Rockel B. Characterization of the rainy season in Burkina Faso and its representation by regional climate models. Climate Dynamics. 2012;39(6):1287–1302. https://doi.org/10.1007/s00382-011-1276-x
56. Lodoun T, Giannini A, Traoré PS, Somé L, Sanon M, Vaksmann M, Rasolodimby JM. Changes in seasonal descriptors of precipitation in Burkina Faso associated with late 20th century drought and recovery in West Africa. Environmental Development. 2013;5:96–108. https://doi.org/10.1016/j.envdev.2012.11.010
57. Sawadogo WL, Zongo G. Processus de prévision, de surveillance et d'alerte précoce de bout en bout à la sécheresse : cas du Burkina Faso [End-to-end drought forecasting, monitoring and early warning process: the case of Burkina Faso]. Paper presented at the regional workshop on end-to-end flood and drought forecasting and early warning. Ouagadougou: Global Water Partnership West Africa; 2023.
58. Burkina Faso. Les conditions de sécheresse et les stratégies de gestion au Burkina Faso [Drought conditions and management strategies in Burkina Faso]. Ouagadougou: Government of Burkina Faso, with the support of WMO, UNCCD, FAO and UNW-DPC; 2015.
59. Biasutti M. Rainfall trends in the African Sahel: characteristics, processes, and causes. WIREs Climate Change. 2019;10(4):e591. https://doi.org/10.1002/wcc.591
60. Mahé G, Paturel J-E. 1896–2006 Sahelian annual rainfall variability and runoff increase of Sahelian Rivers. Comptes Rendus Geoscience. 2009;341(7):538–546. https://doi.org/10.1016/j.crte.2009.05.002
61. Sheffield J, Wood EF, Roderick ML. Little change in global drought over the past 60 years. Nature. 2012;491(7424):435–438. https://doi.org/10.1038/nature11575

62. Dai A. Increasing drought under global warming in observations and models. Nature Climate Change. 2013;3(1):52–58. https://doi.org/10.1038/nclimate1633
63. Roderick ML, Farquhar GD. The cause of decreased pan evaporation over the past 50 years. Science. 2002;298(5597):1410–1411. https://doi.org/10.1126/science.1075390
64. McVicar TR, Roderick ML, Donohue RJ, et al.. Global review and synthesis of trends in observed terrestrial near-surface wind speeds: implications for evaporation. Journal of Hydrology. 2012;416-417:182–205. https://doi.org/10.1016/j.jhydrol.2011.10.024
65. Vicente-Serrano SM, McVicar TR, Miralles DG, Yang Y, Tomas-Burguera M. Unraveling the influence of atmospheric evaporative demand on drought and its response to climate change. WIREs Climate Change. 2020;11(2):e632. https://doi.org/10.1002/wcc.632
66. Ogunrinde AT, Emmanuel I, Olasehinde DA, et al.. Impact of climate teleconnections on hydrological drought in the Sahel Region of Nigeria (SRN). Meteorology and Atmospheric Physics. 2024;136:18. https://doi.org/10.1007/s00703-024-01016-0
67. Di Nunno F, Yildiz MB, Granata F. Decoding the architecture of drought: SHAP-enhanced insights into the climate forces reshaping the Sahel. Hydrology and Earth System Sciences. 2025;29(21):6043–6067. https://doi.org/10.5194/hess-29-6043-2025
68. Ibrahim B, Karambiri H, Polcher J, Yacouba H, Ribstein P. Changes in rainfall regime over Burkina Faso under the climate change conditions simulated by 5 regional climate models. Climate Dynamics. 2014;42(5–6):1363–1381. https://doi.org/10.1007/s00382-013-1837-2
69. Gaetani M, Fontaine B, Roucou P, Baldi M. Influence of the Mediterranean Sea on the West African monsoon: intraseasonal variability in numerical simulations. Journal of Geophysical Research: Atmospheres. 2010;115(D24):D24115. https://doi.org/10.1029/2010JD014436
70. Park J-Y, Bader J, Matei D. Anthropogenic Mediterranean warming essential driver for present and future Sahel rainfall. Nature Climate Change. 2016;6(10):941–945. https://doi.org/10.1038/nclimate3065
71. Diatta S, Fink AH. Statistical relationship between remote climate indices and West African monsoon variability. International Journal of Climatology. 2014;34:3348–3367. https://doi.org/10.1002/joc.3912
72. Camberlin P, Janicot S, Poccard I. Seasonality and atmospheric dynamics of the teleconnection between African rainfall and tropical sea-surface temperature: Atlantic vs. ENSO. International Journal of Climatology. 2001;21(8):973–1005. https://doi.org/10.1002/joc.673
73. Joly M, Voldoire A. Role of the Gulf of Guinea in the inter-annual variability of the West African monsoon: what do we learn from CMIP3 coupled simulations? International Journal of Climatology. 2010;30(12):1843–1856. https://doi.org/10.1002/joc.2026
74. Janicot S, Trzaska S, Poccard I. Summer Sahel-ENSO teleconnection and decadal time scale SST variations. Climate Dynamics. 2001;18(3–4):303–320. https://doi.org/10.1007/s003820100172
75. Giannini A, Saravanan R, Chang P. Oceanic forcing of Sahel rainfall on interannual to interdecadal time scales. Science. 2003;302(5647):1027–1030. https://doi.org/10.1126/science.1089357
76. Joly M, Voldoire A. Influence of ENSO on the West African monsoon: temporal aspects and atmospheric processes. Journal of Climate. 2009;22(12):3193–3210. https://doi.org/10.1175/2008JCLI2450.1
77. Rodríguez-Fonseca B, Janicot S, Mohino E, et al.. Interannual and decadal SST-forced responses of the West African monsoon. Atmospheric Science Letters. 2011;12(1):67–74. https://doi.org/10.1002/asl.308
78. Mohino E, Janicot S, Bader J. Sahel rainfall and decadal to multi-decadal sea surface temperature variability. Climate Dynamics. 2011;37(3–4):419–440. https://doi.org/10.1007/s00382-010-0867-2
79. Martin ER, Thorncroft C. The impact of the AMO on the West African monsoon annual cycle. Quarterly Journal of the Royal Meteorological Society. 2014;140(678):31–46. https://doi.org/10.1002/qj.2107
80. Mahdizadeh J, Ghavidel Y, Farajzadeh M. Spatiotemporal drought variability in Iran and the role of teleconnections. Theoretical and Applied Climatology. 2026;157:709. https://doi.org/10.1007/s00704-026-06638-5